

# Bounds on heat transport for convection driven by internal heating

Ali Arslan<sup>1</sup>†, Giovanni Fantuzzi<sup>1</sup>, John Craske<sup>2</sup> and Andrew Wynn<sup>1</sup>

<sup>1</sup>Department of Aeronautics, Imperial College London

<sup>2</sup>Department of Civil and Environmental Engineering, Imperial College London

(Received xx; revised xx; accepted xx)

The mean vertical heat transport  $\langle wT \rangle$  in convection between isothermal plates driven by uniform internal heating is investigated by means of rigorous bounds. These are obtained as a function of the Rayleigh number  $R$  by constructing feasible solutions to a convex variational problem, derived using a formulation of the classical background method in terms of a quadratic auxiliary function. When the fluid's temperature relative to the boundaries is allowed to be positive or negative, numerical solution of the variational problem shows that best previous bound  $\langle wT \rangle \leq 1/2$  (Goluskin & Spiegel 2012, *Physics Letters A*, vol. 377, pp.83-92) can only be improved up to finite  $R$ . Indeed, we demonstrate analytically that  $\langle wT \rangle \leq 2^{-21/5} R^{1/5}$  and therefore prove that  $\langle wT \rangle < 1/2$  for  $R < 65\,536$ . However, if the minimum principle for temperature is invoked, which asserts that internal temperature is at least as large as the temperature of the isothermal boundaries, then numerically optimised bounds are strictly smaller than  $1/2$  until at least  $R = 3.4 \times 10^5$ . While the computational results suggest that the best bound on  $\langle wT \rangle$  approaches  $1/2$  asymptotically from below as  $R \rightarrow \infty$ , we prove that typical analytical constructions cannot be used to prove this conjecture.

**Key words:** Internally heated convection, turbulent convection, variational methods

## 1. Introduction

Internally-heated (IH) convection, in which the motion of a fluid is driven by buoyancy forces caused by internal sources of heat, is found in a wide variety of natural and built environments, and plays an essential role in disciplines such as geophysics and astrophysics. For example, radioactive decay drives convection in the Earth's mantle, which in turn influences plate tectonics and the planet's magnetic field (Bercovici 2011). A similar mechanism explains geological patterns on the surface of Pluto (Trowbridge *et al.* 2016), and buoyancy flows due to the absorption of solar radiation induce atmospheric turbulence on Venus (Tritton 1975).

Internal heating generalises thermal forcing at the boundaries typical of Rayleigh-Bénard models of convection in both a theoretical and a practical sense, because internal heat sources can be concentrated near boundaries to produce the latter (Bouillaut *et al.* 2019). The dynamics of IH convection are also closely related, and sometimes equivalent, to those of flows driven by internal sources of buoyancy besides temperature, such density stratification due to electromagnetic forces or chemical concentration differences

† Email address for correspondence: a.arslan18@imperial.ac.uk

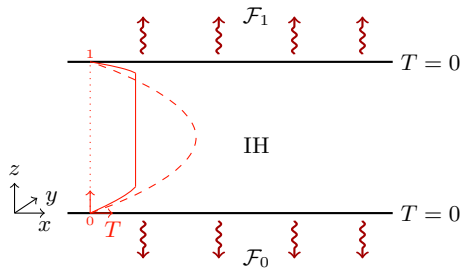


FIGURE 1. Schematic diagram for convection driven by unit uniform internal heat generation, IH, between two isothermal parallel plates. The averaged heat fluxed through the top and bottom plates are denoted by  $\mathcal{F}_1$  and  $\mathcal{F}_0$ , respectively. Red lines illustrate the temperature profile in the conductive regime (---) and a typical mean temperature profile in the turbulent regime (—).

(Goluskin 2016). IH convection therefore warrants study in its own right to enhance fundamental understanding of buoyancy-driven turbulence, yet has received relatively little attention in comparison with Rayleigh–Bénard convection.

A fundamental challenge in the study of IH convection, along with many other turbulent flows, is to characterise the flow’s statistical properties as a function of its control parameters. Following previous work (Goluskin & Spiegel 2012; Goluskin 2016), we consider this problem in the idealized configuration illustrated in Figure 1, where a horizontal layer of fluid between isothermal plates of equal temperature is heated uniformly at a constant rate. The only control parameters for this setting are the Prandtl number of the fluid,  $Pr$ , and the Rayleigh number based on the internal heating rate,  $R$ . Particular statistical quantities of interest are the dimensionless mean temperature,  $\langle T \rangle$ , and the dimensionless mean vertical convective heat flux,  $\langle wT \rangle$ , where the mean is obtained by averaging over volume and infinite time.

The dimensionless mean temperature  $\langle T \rangle$  corresponds to the amount of thermal dissipation in the fluid and can be related qualitatively to the proportion of heat within the fluid that is transported by conduction, rather than by convection. As described by Goluskin & Spiegel (2012, p.87), the average outward conduction above and below the plane over which the time- and plane-averaged temperature  $\bar{T}$  is maximised is equal to  $2\bar{T}$ . If one assumes that at high  $R$  the temperature field is well mixed, then  $\langle T \rangle$  scales in the same way as the maximum of  $\bar{T}$ . The ratio of the total (predominantly convective) heat flux to the conductive heat flux, which corresponds to a Nusselt number, is therefore  $1/(2\bar{T}) \sim 1/\langle T \rangle$ . In contrast,  $\langle wT \rangle$  quantifies the vertical asymmetry caused by the fluid’s motion and is related to the heat fluxes  $\mathcal{F}_1$  and  $\mathcal{F}_0$  through the top and bottom boundaries by the exact relations (Goluskin 2016)

$$\mathcal{F}_1 = \frac{1}{2} + \langle wT \rangle, \quad \mathcal{F}_0 = \frac{1}{2} - \langle wT \rangle. \quad (1.1)$$

Laboratory experiments (Kulacki & Goldstein 1972; Jahn & Reineke 1974; Mayinger *et al.* 1976; Kakac *et al.* 1985; Lee *et al.* 2007) and direct numerical simulations (Peckover & Hutchinson 1974; Straus 1976; Tveitereid 1978; Emara & Kulacki 1980; Wörner *et al.* 1997; Goluskin & Spiegel 2012; Goluskin & van der Poel 2016) indicate that the dimensional mean temperature increases sublinearly with the heating rate, which, in nondimensional terms, implies that  $\langle T \rangle$  decreases with  $R$ . Scaling arguments for Rayleigh–Bénard convection (Grossmann & Lohse 2000) can be applied to the top boundary layer of IH convection (Goluskin & Spiegel 2012; Wang *et al.* 2020) and imply that  $\langle T \rangle \sim Pr^{-1/3} R^{-1/3}$  when  $Pr \lesssim R^{-1/4}$  and  $\langle T \rangle \sim R^{-1/4}$  otherwise. The dependence

of these predictions on the Rayleigh number agrees with rigorous lower bounds on  $\langle T \rangle$  for both finite and infinite  $Pr$  (Lu *et al.* 2004; Whitehead & Doering 2011a) up to logarithmic corrections. However, as mentioned in Goluskin & Spiegel (2012) and discussed in §3 of this paper, understanding the scaling of  $\langle wT \rangle$  in IH convection requires additional information pertaining to the bottom boundary layer.

In contrast to  $\langle T \rangle$ , the behaviour of the mean vertical convective heat flux  $\langle wT \rangle$  remains fascinatingly unclear. While  $\langle wT \rangle$  appears to increase with  $R$  in experiments (Kulacki & Goldstein 1972) and three-dimensional simulations (Goluskin & van der Poel 2016), it displays little variation with respect to  $R$  and non-monotonic behaviour in two-dimensional simulations (Goluskin & Spiegel 2012; Wang *et al.* 2020). Power-law fits to experimental and numerical data summarised by Goluskin (2016) suggest that

$$\langle wT \rangle \approx \frac{1}{2} - \sigma R^{-\alpha}, \quad (1.2)$$

with prefactors  $\sigma \approx 1$  and exponents  $\alpha$  between 0.05 and 0.1. Physical theories corroborating this power-law behaviour are lacking and the best rigorous mathematical result available to date is the uniform bound  $\langle wT \rangle \leq 1/2$  (Goluskin & Spiegel 2012).

This work reports new  $R$ -dependent upper bounds on  $\langle wT \rangle$ , some obtained computationally and some proved analytically, the derivation of which relies on two key ingredients. The first is a modern interpretation of the background method (Constantin & Doering 1995; Doering & Constantin 1994, 1996) as a particular case of a broader framework for bounding infinite-time averages (Chernyshenko *et al.* 2014; Fantuzzi *et al.* 2016; Chernyshenko 2017; Tobiasco *et al.* 2018; Goluskin & Fantuzzi 2019; Rosa & Temam 2020). This interpretation makes it possible to formulate a variational bounding principle for  $\langle wT \rangle$  even though, contrary to most past applications of the background method to convection problems (Doering & Constantin 1996; Constantin & Doering 1996; Doering & Constantin 1998; Constantin & Doering 1999; Doering & Constantin 2001; Otero *et al.* 2002; Yan 2004; Otero *et al.* 2004; Doering *et al.* 2006; Whitehead & Doering 2011b, 2012; Goluskin 2015; Goluskin & Doering 2016), this quantity is not directly related to the thermal dissipation. The second key ingredient is a minimum principle, already invoked by Goluskin & Spiegel (2012) and proved in Appendix A, stating that the temperature of the fluid is either no smaller than that of the top and bottom plates, or approaches such a state exponentially quickly. Similar results have proved extremely useful in the context of Rayleigh–Bénard convection (Constantin & Doering 1999; Yan 2004; Otto & Seis 2011; Goluskin & Doering 2016; Choffrut *et al.* 2016) and, as we shall demonstrate, appear essential for proving  $R$ -dependent bounds on  $\langle wT \rangle$  for IH convection at large  $R$ .

The rest of this work is structured as follows. Section 2 describes the flow configuration and the corresponding governing equations. Heuristic scaling arguments for the mean vertical heat flux are presented in §3. In §4, we derive two variational principles to bound  $\langle wT \rangle$  rigorously from above: one that does not consider the minimum principle for the temperature, and one that enforces it by means of a Lagrange multiplier. Computational and analytical bounds obtained with the former are presented in §5, while bounds obtained numerically with the latter are discussed in §6, along with obstacles to analytical constructions. Section 7 offers concluding remarks.

Throughout the paper, overlines indicate averages over the horizontal directions and infinite time, while angled brackets denote averages over the dimensionless volume  $\Omega = [0, L_x] \times [0, L_y] \times [0, 1]$  and infinite time. Precisely, for any scalar-valued function  $f(\mathbf{x}, t)$ ,

$$\bar{f} = \limsup_{\tau \rightarrow \infty} \frac{1}{\tau L_x L_y} \int_0^\tau \int_0^{L_x} \int_0^{L_y} f(\mathbf{x}, t) \, dx \, dy \, dt, \quad (1.3a)$$

$$\langle f \rangle = \limsup_{\tau \rightarrow \infty} \frac{1}{\tau} \int_0^\tau \int_\Omega f(\mathbf{x}, t) \, d\mathbf{x} \, dt, \quad (1.3b)$$

where  $f_\Omega(\cdot) d\mathbf{x} = (L_x L_y)^{-1} \int_\Omega (\cdot) d\mathbf{x}$  is the spatial average. Note that  $\bar{f} = \bar{f}(z)$  depends only on the vertical coordinate  $z$ . We also write  $\|f\|_2$  and  $\|f\|_\infty$  for the usual  $L^2$  and  $L^\infty$  norms of univariate functions  $f(z)$  on the interval  $[0, 1]$ . Derivatives of univariate functions with respect to  $z$  will be denoted by primes.

## 2. Governing equations

We consider a layer of fluid confined between two no-slip plates that are separated by a vertical distance  $d$  and are held at the same constant temperature, which may be taken to be zero without loss of generality. The fluid has density  $\rho$ , kinematic viscosity  $\nu$ , thermal diffusivity  $\kappa$ , thermal expansion coefficient  $\alpha$ , specific heat capacity  $c_p$ , and is heated uniformly at a volumetric rate  $Q$ . This corresponds to the configuration denoted by IH1 in Goluskin (2016). To simplify the discussion we assume that the layer is periodic in the horizontal ( $x$  and  $y$ ) directions with periods  $L_x d$  and  $L_y d$ , but all results presented in §5 and §6 will be independent of the domain aspect ratios  $L_x$  and  $L_y$ .

To make the problem nondimensional we use  $d$  as the length scale,  $d^2/\kappa$  as the time scale and  $d^2 Q/\kappa$  as the temperature scale. Under the Boussinesq approximation, the Navier–Stokes equations governing the motion of the fluid in the nondimensional domain  $\Omega = [0, L_x] \times [0, L_y] \times [0, 1]$  are (Goluskin 2016)

$$\nabla \cdot \mathbf{u} = 0, \quad (2.1a)$$

$$\partial_t \mathbf{u} + \mathbf{u} \cdot \nabla \mathbf{u} + \nabla p = Pr(\nabla^2 \mathbf{u} + RT\hat{\mathbf{z}}), \quad (2.1b)$$

$$\partial_t T + \mathbf{u} \cdot \nabla T = \nabla^2 T + 1, \quad (2.1c)$$

with boundary conditions

$$\mathbf{u}|_{z=0} = \mathbf{u}|_{z=1} = 0, \quad (2.2a)$$

$$T|_{z=0} = T|_{z=1} = 0. \quad (2.2b)$$

The dimensionless Prandtl and Rayleigh numbers are defined as

$$Pr = \frac{\nu}{\kappa}, \quad R = \frac{g\alpha Q d^5}{\rho c_p \nu \kappa^2}. \quad (2.3)$$

The former measures the ratio of momentum and heat diffusivity and is a property of the fluid, while the latter measures the destabilising effect of internal heating compared with the stabilising effect of diffusion and is the control parameter in this study.

For any value of  $R$  and  $Pr$ , equations (2.1a–c) admit the steady solution,  $\mathbf{u} = \mathbf{0}$ ,  $T = \frac{1}{2}z(1-z)$ , which represents a purely conductive state. This solution is globally asymptotically stable for any values of the horizontal periods  $L_x$  and  $L_y$  when  $R < 26\,926$  (Goluskin 2016) and is linearly unstable when  $R$  is larger than a critical threshold  $R_L \approx 37\,325$  (Debler 1959), the exact value of which depends on the horizontal periods. Sustained convection ensues in this regime, but has also been observed at subcritical Rayleigh numbers (Tveitereid 1978). Our goal is to characterize the mean vertical convective heat flux through the layer,  $\langle wT \rangle$ , as a function of  $R$ .

### 3. Heuristic scaling arguments

Phenomenological predictions for the variation of  $\langle wT \rangle$  with the Rayleigh number can be derived by coupling the total heat budget through the layer with scaling assumptions for characteristic length scales  $\delta_T$  and  $\varepsilon_T$  of the lower and upper thermal boundary layers, respectively. These length scales can be defined such that  $\langle T \rangle / \delta_T = \mathcal{F}_0$  and  $\langle T \rangle / \varepsilon_T = \mathcal{F}_1$ . Averaging (2.1c) over space and infinite time indicates that  $\delta_T$  and  $\varepsilon_T$  satisfy

$$\frac{\langle T \rangle}{\delta_T} + \frac{\langle T \rangle}{\varepsilon_T} = 1, \quad (3.1)$$

while the second identity in (1.1) yields

$$\langle wT \rangle = \frac{1}{2} - \frac{\langle T \rangle}{\delta_T}. \quad (3.2)$$

For the sake of definiteness, assume that the mean temperature and  $\delta_T$  decay as power laws in  $R$ , that is,  $\langle T \rangle = R^{-\alpha_0} / \sigma_0$  and  $\delta_T = R^{-\alpha_1} / \sigma_1$  with  $\alpha_0, \alpha_1 \geq 0$ . If  $\langle wT \rangle$  approaches a constant as  $R$  is raised, then  $\langle T \rangle \leq O(\delta_T)$  and  $\alpha_1 \leq \alpha_0$ , the inequality being strict if  $\langle wT \rangle \rightarrow 1/2$ . Moreover, (3.1) implies that

$$\frac{1}{\varepsilon_T} = \sigma_0 R^{\alpha_0} - \sigma_1 R^{\alpha_1}. \quad (3.3)$$

The scalings behind IH convection with the isothermal boundary conditions (2.2) are therefore necessarily subtle, because the leading scaling of  $\varepsilon_T$  (hence, of  $\langle T \rangle$ ) and the correction implied by  $\delta_T$  both play a crucial role. Any heuristic argument therefore needs to distinguish between the physics associated with the unstably stratified flow near the upper boundary from the (very different) stably stratified flow near the lower boundary. In particular, one must determine whether  $\langle T \rangle$  reduces at the same rate as  $\delta_T$ , meaning that  $\langle wT \rangle$  tends to a constant value in the range  $[0, 1/2)$  determined by the relative magnitude of the prefactors  $\sigma_0$  and  $\sigma_1$ , or slightly faster, implying that  $\langle wT \rangle$  approaches  $1/2$  as the Rayleigh number is raised.

As noted by Whitehead & Doering (2011a), one way to derive a scaling for  $\varepsilon_T$  is to assume that the upper boundary layer maintains a state of marginal stability (Malkus 1954; Priestley 1954). In this case,  $\varepsilon_T$  adjusts itself such that the local Rayleigh number  $Ra_{\varepsilon_T}$ , based on the average temperature and depth of the upper boundary layer, remains constant. Expressing  $Ra_{\varepsilon_T}$  in terms of  $R$  to leading order, we conclude that

$$Ra_{\varepsilon_T} = \langle T \rangle \varepsilon_T^3 R \sim \sigma_0^4 R^{1-4\alpha_0}, \quad (3.4)$$

should be independent of  $R$ , which implies that  $\alpha_0 = 1/4$ , as noted by (Goluskin & Spiegel 2012, Table 2) and consistent with the scalings proposed by Wang *et al.* (2020, see regimes III $_{\infty}$  and IV $_u$ ). Alternatively, if one uses an argument based on balancing a characteristic free-fall velocity  $\sqrt{PrR\langle T \rangle}$  with the velocity scale  $1/\varepsilon_T$  implied by diffusion at the wall (Spiegel 1963), then to leading order

$$\varepsilon_T \sqrt{PrR\langle T \rangle} \sim \sigma_0^{\frac{3}{2}} Pr^{\frac{1}{2}} R^{1-3\alpha_0}, \quad (3.5)$$

is independent of  $R$ , implying that  $\alpha_0 = 1/3$ . In either case ( $\alpha_0 = 1/4$  or  $\alpha_0 = 1/3$ ), the resulting scaling corresponds to the first term in the asymptotic expansion of  $\varepsilon_T$  and does not provide any information about the correction due to  $\delta_T$ , which is crucial to determine the asymptotic behaviour of  $\langle wT \rangle$ .

The simplest argument relating to  $\delta_T$ , although not necessarily the most faithful, comes from assuming that in some vicinity of the lower boundary there is a balance between heating and diffusion because the flow is stably stratified. In terms of the dimensionless

variables used here, heating over  $\delta_T$  is proportional to  $\delta_T$  and diffusion is equal to  $\langle T \rangle / \delta_T$ , which implies that  $\delta_T^2 \sim \langle T \rangle$ . This requires  $\alpha_1 = \alpha_0/2$ , leading to  $\alpha_1 = 1/8$  or  $\alpha_1 = 1/6$  for scaling of  $\varepsilon_T$  based on Malkus (1954) or Spiegel (1963), respectively, and therefore to  $\langle wT \rangle = 1/2 - \sigma_1 R^{-\frac{1}{8}} / \sigma_0$  or  $\langle wT \rangle = 1/2 - \sigma_1 R^{-\frac{1}{6}} / \sigma_0$ . Assuming that  $\max(\overline{T})$  scales in the same way as  $\langle T \rangle$ , meaning that the average temperature is approximately uniform away from boundaries, the possibility that  $\delta_T^2 \sim \langle T \rangle$  (so  $\alpha_1 = \alpha_0/2$ ) is in reasonably good agreement with data from experiments and simulations (Goluskin 2016, table 3.2).

An alternative argument might consider a Richardson number  $Ri$  at the lower boundary layer to quantify the destabilising effects of turbulence relative to the stabilising effects of the density stratification. In terms of dimensionless quantities, the density stratification is  $\langle T \rangle / \delta_T$  and we assume that the destabilising shear across the lower boundary scales according to  $\sqrt{\langle T \rangle} / \delta_T$ . Together, these scales imply that  $Ri \sim \delta_T$ . This is significant because, if the flow tends towards a state of marginal stability, then  $Ri = 1/4$  according to the Miles–Howard criterion for steady, laminar, parallel and inviscid shear flow (Miles 1961; Howard 1961). We would therefore conclude that either  $\langle wT \rangle = 1/2 - \sigma_1 R^{-\frac{1}{4}} / \sigma_0$  or  $\langle wT \rangle = 1/2 - \sigma_1 R^{-\frac{1}{3}} / \sigma_0$ , corresponding to Malkus (1954) or Spiegel (1963) respectively. The latter scaling would be consistent with the conjectured bound for insulating lower boundary conditions, but, unlike the scaling argument outlined in the previous paragraph, is far from the wide range of scaling possibilities that have been inferred from experiments and simulations (Goluskin 2016). Indeed, available data is too scattered to provide conclusive information about the asymptotic behaviour of  $\langle wT \rangle$ , highlighting the need for further experiments and simulations in addition to the rigorous bounds pursued here.

## 4. Formulation of rigorous bounds

We now turn our attention to bounding  $\langle wT \rangle$  rigorously from above. In §§4.1–4.3 we ignore the minimum principle for the temperature field and our analysis can be seen as a “classical” application of the background method. In §4.4, instead, we improve the analysis by taking the minimum principle into account through a Lagrange multiplier.

### 4.1. Bounds via auxiliary functional

A rigorous upper bound on  $\langle wT \rangle$  can be derived using the simple observation that the infinite-time average of the time derivative of any bounded function  $\mathcal{V}\{\mathbf{u}, T\}$  along solutions of the governing equations (2.1a–c) vanishes, so

$$\langle wT \rangle = \limsup_{\tau \rightarrow \infty} \frac{1}{\tau} \int_0^\tau \left[ \int_\Omega wT + \frac{d}{dt} \mathcal{V}\{\mathbf{u}, T\} \, d\mathbf{x} \right] dt. \quad (4.1)$$

In particular, if  $\mathcal{V}$  can be chosen such that

$$\mathcal{S}\{\mathbf{u}, T\} := U - \int_\Omega wT + \frac{d}{dt} \mathcal{V}\{\mathbf{u}, T\} \, d\mathbf{x} \geq 0 \quad (4.2)$$

for all time along solutions of (2.1a–c) for some constant  $U$ , then  $\langle wT \rangle \leq U$ . The goal, then, is to construct  $\mathcal{V}$  that satisfies (4.2) with the smallest possible  $U$ .

While the evolution equations (2.1b) and (2.1c) cannot be solved explicitly for all possible initial conditions, when  $\mathcal{V}$  is given they can be used to derive an explicit expression for  $\mathcal{S}$  as a function of  $\mathbf{u}$  and  $T$  alone. Then, to ensure that (4.2) holds along solutions (2.1a–c) pointwise in time, it suffices to enforce that  $\mathcal{S}\{\mathbf{u}, T\}$  be nonnegative when viewed as a functional on the space of time-independent incompressible velocity

fields and temperature fields that satisfy the boundary conditions,

$$\mathcal{H} := \{(\mathbf{u}, T) : (2.2a,b), \text{ horizontal periodicity and } \nabla \cdot \mathbf{u} = 0\}. \quad (4.3)$$

We therefore search for a function  $\mathcal{V}$  and constant  $U$  such that  $\mathcal{S}\{\mathbf{u}, T\} \geq 0$  for all velocity and temperature fields in  $\mathcal{H}$ . This key relaxation makes this approach tractable and, remarkably, it may not be overly conservative. In fact, if the governing equations in (2.1) were well posed (which is not currently known) and solutions eventually remained in a compact subset  $\mathcal{K}$  of  $\mathcal{H}$ , then optimizing  $\mathcal{V}$  over a sufficiently general class of functions whilst imposing  $\mathcal{S}\{\mathbf{u}, T\} \geq 0$  for all  $\mathbf{u}$  and  $T$  in  $\mathcal{K}$ , would yield an upper bound  $U$  exactly equal to the largest possible value of  $\langle wT \rangle$  (Rosa & Temam 2020).

Unfortunately, the construction of such an optimal  $\mathcal{V}$  is currently beyond the reach of both analytical and computational methods. Nevertheless, progress can be made if we restrict the search to quadratic  $\mathcal{V}$  in the form

$$\mathcal{V}\{\mathbf{u}, T\} = \int_{\Omega} \frac{a}{2PrR} |\mathbf{u}|^2 + \frac{b}{2} |T|^2 - [\psi(z) + z - 1] T \, d\mathbf{x}, \quad (4.4)$$

where the nonnegative scalars  $a$  and  $b$  and the function  $\psi(z)$  are to be optimized such that (4.2) holds for the smallest possible  $U$ . As shown by Chernyshenko (2017), this choice of  $\mathcal{V}$  amounts to using the background method (Constantin & Doering 1995; Doering & Constantin 1994, 1996): the profile  $\frac{1}{b}[\psi(z) + z - 1]$  corresponds to the background temperature field, while the scalars  $a$  and  $b$  are the so-called balance parameters. Note that the  $z-1$  term could be removed by redefining  $\psi(z)$ , but we isolate it to simplify the analysis in what follows. Note also that, due to the periodicity in the horizontal directions, a ‘‘symmetry reduction’’ argument following ideas in Goluskin & Fantuzzi (2019, Appendix A) proves that there is no loss of generality in taking  $\psi$  to depend only on the vertical coordinate  $z$ . Similarly, one can show that the upper bound on  $\langle wT \rangle$  cannot be improved by adding to  $\mathcal{V}$  a term  $\phi \cdot \mathbf{u}$ , proportional to the velocity field via a (rescaled) incompressible background velocity field  $\phi$ .

To find an expression for  $\mathcal{S}\{\mathbf{u}, T\}$ , we calculate the time derivative of the quadratic  $\mathcal{V}$  in (4.4) using the governing equations (2.1b,c), substitute the resulting expression into (4.2), and integrate various terms by parts using incompressibility and the boundary conditions (2.2a,b) to arrive at

$$\begin{aligned} \mathcal{S}\{\mathbf{u}, T\} = \int_{\Omega} \left[ \frac{a}{R} |\nabla \mathbf{u}|^2 + b |\nabla T|^2 - (a - \psi') wT + (bz - \psi' - 1) \partial_z T + \psi \right] d\mathbf{x} \\ + \psi(1) \overline{T}'(1) - (\psi(0) - 1) \overline{T}'(0) + U - \frac{1}{2}. \end{aligned} \quad (4.5)$$

The best bound on  $\langle wT \rangle$  that can be proved with quadratic  $\mathcal{V}$  is

$$\langle wT \rangle \leq \inf_{U, \psi(z), a, b} \{U : \mathcal{S}\{\mathbf{u}, T\} \geq 0 \, \forall (\mathbf{u}, T) \in \mathcal{H}\}. \quad (4.6)$$

The right-hand side of (4.6) is a linear optimisation problem because the optimisation variables,  $U$ ,  $\psi(z)$ ,  $a$  and  $b$ , enter the constraint  $\mathcal{S}\{\mathbf{u}, T\} \geq 0$  and the cost  $U$  linearly.

#### 4.2. Fourier expansion

The analysis and numerical implementation of the minimisation problem in (4.6) can be considerably simplified by expanding the horizontally-periodic velocity and temperature as Fourier series,

$$\begin{bmatrix} T(x, y, z) \\ \mathbf{u}(x, y, z) \end{bmatrix} = \sum_{\mathbf{k}} \begin{bmatrix} \hat{T}_{\mathbf{k}}(z) \\ \hat{\mathbf{u}}_{\mathbf{k}}(z) \end{bmatrix} e^{i(k_x x + k_y y)}. \quad (4.7)$$



The sums are over wavevectors  $\mathbf{k} = (k_x, k_y)$  compatible with the horizontal periods  $L_x$  and  $L_y$ . We denote the magnitude of each wavevector by  $k = \sqrt{k_x^2 + k_y^2}$ . The complex-valued Fourier amplitudes satisfy the complex-conjugate relations  $\hat{\mathbf{u}}_{-\mathbf{k}} = \hat{\mathbf{u}}_{\mathbf{k}}^*$  and  $\hat{T}_{-\mathbf{k}} = \hat{T}_{\mathbf{k}}^*$ , as well as the no-slip and isothermal boundary conditions. Using incompressibility and writing  $\hat{w}_{\mathbf{k}}$  for the vertical component of  $\hat{\mathbf{u}}_{\mathbf{k}}$ , these can be expressed as

$$\hat{w}_{\mathbf{k}}(0) = \hat{w}'_{\mathbf{k}}(0) = \hat{w}_{\mathbf{k}}(1) = \hat{w}'_{\mathbf{k}}(1) = 0, \quad (4.8a)$$

$$\hat{T}_{\mathbf{k}}(0) = \hat{T}_{\mathbf{k}}(1) = 0. \quad (4.8b)$$

After inserting the Fourier expansions (4.7) into (4.5) and applying standard estimates based on the incompressibility condition and Young's inequality to replace the horizontal Fourier amplitudes  $\hat{u}_{\mathbf{k}}$  and  $\hat{v}_{\mathbf{k}}$  as a function of  $\hat{w}_{\mathbf{k}}$ , the functional  $\mathcal{S}\{\mathbf{u}, T\}$  can be estimated from below as

$$\mathcal{S}\{\mathbf{u}, T\} \geq \mathcal{S}_0\{\hat{T}_0\} + \sum_{\mathbf{k}} \mathcal{S}_{\mathbf{k}}\{\hat{w}_{\mathbf{k}}, \hat{T}_{\mathbf{k}}\}, \quad (4.9)$$

where

$$\mathcal{S}_0\{\hat{T}_0\} = \int_0^1 \left[ b|\hat{T}'_0|^2 + (bz - \psi')\hat{T}'_0 + \psi \right] dz + \psi(1)\hat{T}'_0(1) - (\psi(0) - 1)\hat{T}'_0(0) + U - \frac{1}{2} \quad (4.10)$$

and

$$\begin{aligned} \mathcal{S}_{\mathbf{k}}\{\hat{w}_{\mathbf{k}}, \hat{T}_{\mathbf{k}}\} = \int_0^1 \left[ \frac{a}{R} \left( \frac{1}{k^2} |\hat{w}''_{\mathbf{k}}|^2 + 2|\hat{w}'_{\mathbf{k}}|^2 + k^2 |\hat{w}_{\mathbf{k}}|^2 \right) \right. \\ \left. + b|\hat{T}'_{\mathbf{k}}|^2 + bk^2|\hat{T}_{\mathbf{k}}|^2 - (a - \psi')\hat{w}_{\mathbf{k}}\hat{T}_{\mathbf{k}}^* \right] dz. \quad (4.11) \end{aligned}$$

Equality holds in (4.9) if  $\mathbf{u}$  has only one nonzero horizontal component because, in this case, the Fourier-transformed incompressibility condition yields an exact relation between  $\hat{w}_{\mathbf{k}}$  and either  $\hat{u}_{\mathbf{k}}$  or  $\hat{v}_{\mathbf{k}}$ , so Young's inequality is not needed to eliminate the latter.

Velocity and temperature fields with a single nonzero Fourier mode are admissible in the optimization problem (4.6), so the right-hand side of (4.9) is nonnegative if and only if each term is nonnegative. Moreover, since the real and imaginary parts of the Fourier amplitudes  $\hat{w}_{\mathbf{k}}$  and  $\hat{T}_{\mathbf{k}}$  give identical and independent contributions to  $\mathcal{S}_{\mathbf{k}}$ , we may assume them to be real without loss of generality. Thus, we may replace the minimization problem in (4.6) with

$$\begin{aligned} & \inf_{U, \psi(z), a, b} U \\ & \text{subject to } \mathcal{S}_0\{\hat{T}_0\} \geq 0 \quad \forall \hat{T}_0 : (4.8b), \\ & \mathcal{S}_{\mathbf{k}}\{\hat{w}_{\mathbf{k}}, \hat{T}_{\mathbf{k}}\} \geq 0 \quad \forall \hat{w}_{\mathbf{k}}, \hat{T}_{\mathbf{k}} : (4.8a, b), \quad \forall \mathbf{k} \neq 0. \end{aligned} \quad (4.12)$$

Any choice of  $U$ ,  $\psi(z)$ ,  $a$  and  $b$  satisfying the constraints yields a rigorous upper bound on the mean vertical convective heat flux  $\langle wT \rangle$ . Following established terminology, we refer to the inequalities on  $\mathcal{S}_{\mathbf{k}}$  as the spectral constraints.

Just like (4.6), the optimization problem in (4.12) is linear and its optimal solution can be approximated using efficient numerical algorithms after discretization. For computational convenience, however, we simplify the spectral constraints by dropping all nonnegative terms that depend explicitly on  $k$ . Specifically, we replace the spectral constraints with the stronger, but simpler, single condition

$$\tilde{\mathcal{S}}\{\hat{w}, \hat{T}\} := \int_0^1 \frac{2a}{R} |\hat{w}'|^2 + b|\hat{T}'|^2 - (a - \psi')\hat{w}\hat{T} dz \geq 0 \quad \forall \hat{T}, \hat{w} : (4.8a, b) \quad (4.13)$$



and solve

$$\begin{aligned} & \inf_{U, \psi(z), a, b} U \\ \text{subject to } & \mathcal{S}_0\{\hat{T}_0\} \geq 0 \quad \forall \hat{T}_0 : (4.8b), \\ & \tilde{\mathcal{S}}\{\hat{w}, \hat{T}\} \geq 0 \quad \forall \hat{w}, \hat{T} : (4.8a, b) \end{aligned} \quad (4.14)$$

instead of (4.12). This simplification leads to suboptimal bounds on  $\langle wT \rangle$  at a fixed  $R$  but, as discussed in Appendix B, still captures the qualitative behaviour of the optimal ones. On the other hand, considering the simplified spectral constraint (4.13) allows for significant computational savings when optimizing bounds numerically, because it removes the need to consider a large set of wavenumbers and it enables implementation using simple piecewise-linear basis functions (cf. appendix D). This allows for discretization of (4.14) and its generalization (4.25) derived in §4.4 below on very fine meshes, which is essential to resolve sharp boundary layers in  $\psi$  accurately.

### 4.3. Explicit formulation

To simplify the analysis (but not the numerical implementation) of (4.12) it is convenient to eliminate the explicit appearance of  $U$ . This can be done upon observing that, given any profile  $\psi(z)$  and balance parameters  $a, b$ , the smallest  $U$  for which  $\mathcal{S}_0\{\hat{T}_0\}$  is nonnegative over admissible  $\hat{T}_0$  is

$$U^* = \frac{1}{2} + \sup_{\substack{\hat{T}_k(0)=0 \\ \hat{T}_k(1)=0}} \left\{ - \int_0^1 \left[ b|\hat{T}'_0|^2 + (bz - \psi')\hat{T}'_0 + \psi \right] dz - \psi(1)\hat{T}'_0(1) + (\psi(0) - 1)\hat{T}'_0(0) \right\}. \quad (4.15)$$

By modifying any admissible  $\hat{T}_0$  in infinitesimally thin layers near  $z = 0$  and  $z = 1$ , it is possible to show that this value is finite if and only if

$$\psi(0) = 1 \quad \text{and} \quad \psi(1) = 0. \quad (4.15a, b)$$

Then, the optimal temperature field in (4.15) is given by

$$\hat{T}'_0(z) = \frac{\psi'(z) + 1}{2b} - \frac{z}{2} + \frac{1}{4}, \quad (4.16)$$

and we obtain

$$U^* = \frac{1}{2} + \frac{1}{4b} \left\| bz - \frac{b}{2} - \psi'(z) - 1 \right\|_2^2 - \int_0^1 \psi dz. \quad (4.17)$$

Thus, we may replace the minimization problem (4.12) with the more explicit version

$$\begin{aligned} & \inf_{\psi(z), a, b} \frac{1}{2} + \frac{1}{4b} \left\| bz - \frac{b}{2} - \psi'(z) - 1 \right\|_2^2 - \int_0^1 \psi dz \\ \text{subject to } & \psi(0) = 1, \\ & \psi(1) = 0, \\ & \mathcal{S}_k\{\hat{w}, \hat{T}\} \geq 0 \quad \forall \hat{w}, \hat{T} : (4.8a, b). \end{aligned} \quad (4.18)$$

Note that although this formulation is not suitable for numerical implementation because the cost function is not convex with respect to  $b$ , it is more convenient when attempting to prove an upper bound on  $\langle wT \rangle$  analytically.

#### 4.4. Restriction to nonnegative temperature fields

The upper bounding principle derived above can be improved by imposing a minimum principle, which guarantees that temperature fields solving the Boussinesq equations (2.1a–c) are nonnegative in the domain  $\Omega$  at large time. More precisely, Appendix A proves that the fluid's temperature is nonnegative on  $\Omega$  at all times if it is so initially, and the negative part of the temperature decays exponentially quickly otherwise.

Since  $\langle wT \rangle$  is determined by the long-time behaviour of the velocity and temperature fields, the minimum principle enables us to replace the upper bound (4.6) with

$$\langle wT \rangle \leq \inf_{U, \psi(z), a, b} \{U : \mathcal{S}\{\mathbf{u}, T\} \geq 0 \quad \forall (\mathbf{u}, T) \in \mathcal{H}_+\}, \quad (4.19)$$

where the space  $\mathcal{H}$  of admissible velocity and temperature fields has been replaced with its subset

$$\mathcal{H}_+ := \{(\mathbf{u}, T) \in \mathcal{H} : T(\mathbf{x}) \geq 0 \text{ on } \Omega\}. \quad (4.20)$$

The constraint in the modified optimisation problem (4.19) is clearly weaker than the original one in (4.6), so imposing the minimum principle allows for a better bound on  $\langle wT \rangle$  in principle. This is indeed the case at large Rayleigh numbers, as shall be demonstrated by numerical results in §5 and §6.

In order to impose the inequality constraint  $\mathcal{S}\{\mathbf{u}, T\} \geq 0$  for nonnegative temperatures, but relax it when  $T$  is negative on a nonnegligible subset of the domain, we effectively use a Lagrange multiplier. Specifically, we search for a positive bounded linear functional  $\mathcal{L}$  such that  $\mathcal{S}\{\mathbf{u}, T\} \geq \mathcal{L}\{T\}$  for all pairs  $(\mathbf{u}, T) \in \mathcal{H}$ , which satisfy only the boundary condition and incompressibility. Indeed, the positivity of  $\mathcal{L}$  implies  $\mathcal{S}\{\mathbf{u}, T\} \geq \mathcal{L}\{T\} \geq 0$  if  $T$  is nonnegative, as desired. When  $T$  is negative on a subset of the domain, instead,  $\mathcal{L}\{T\}$  need not be positive and the constraint on  $\mathcal{S}\{\mathbf{u}, T\}$  is relaxed.

Analysis in Appendix C proves that there is no loss of generality in taking

$$\mathcal{L}\{T\} = - \int_{\Omega} q(z) \partial_z T \, d\mathbf{x}, \quad (4.21)$$

where  $q : (0, 1) \rightarrow \mathbb{R}$  is a nondecreasing function, square-integrable but not necessarily continuous, to be optimised alongside the bound  $U$ , the profile  $\psi(z)$ , and the balance parameter  $a, b$ . If  $q$  were differentiable, one could integrate by parts to obtain

$$\mathcal{L}\{T\} = \int_{\Omega} q'(z) T \, d\mathbf{x} \quad (4.22)$$

and identify  $q'$  as a standard Lagrange multiplier for the condition  $T(\mathbf{x}) \geq 0$ ; working with (4.21) simply removes the differentiability requirement from  $q$ . Moreover, the value of  $\mathcal{L}\{T\}$  in (4.21) does not change when  $q$  is shifted by a constant by virtue of the vertical boundary conditions on  $T$ , so we may normalize  $q$  such that

$$\int_0^1 q(z) \, dz = \psi(1) - \psi(0). \quad (4.23)$$

The upper bound (4.19) can therefore be replaced with

$$\langle wT \rangle \leq \inf_{U, \psi(z), q(z), a, b} \left\{ U : q(z) \text{ nondecreasing, (4.23) and} \right. \\ \left. \mathcal{S}\{\mathbf{u}, T\} + \int_{\Omega} q(z) \partial_z T \, d\mathbf{x} \geq 0 \quad \forall (\mathbf{u}, T) \in \mathcal{H}, \right\}. \quad (4.24)$$

Observe that setting  $q(z) = -1$  causes the integral  $\int_{\Omega} q(z) \frac{\partial T}{\partial z} dx$  to vanish because  $T$  is zero at the top and bottom boundaries, so this choice of  $q$  results in the upper bound (4.6) derived without the minimum principle for  $T$ .

The minimisation problem in (4.24) can be expanded using a Fourier series exactly as explained in §4.2. After estimating the functionals  $\mathcal{S}_k$  with  $\tilde{\mathcal{S}}$ , one concludes that  $\langle wT \rangle$  is bounded above by the optimal value of the following linear optimization problem:

$$\begin{aligned} & \inf_{U, a, b, \psi(z), q(z)} U \\ \text{subject to } & \mathcal{S}_0\{\hat{T}_0\} + \int_0^1 q(z) \hat{T}'_0(z) dz \geq 0 \quad \forall \hat{T}_0 : \hat{T}_0(0) = 0 = \hat{T}_0(1), \quad (4.25) \\ & \tilde{\mathcal{S}}\{\hat{w}, \hat{T}\} \geq 0 \quad \forall \hat{w}, \hat{T} : (4.8a, b), \\ & q(z) \text{ nondecreasing.} \end{aligned}$$

If one does not simplify the spectral constraints, one obtains a very similar problem where the inequality on  $\tilde{\mathcal{S}}$  is replaced by the same  $k$ -dependent inequalities appearing in (4.12). This problem gives a quantitatively better bound on  $\langle wT \rangle$  but has a higher computational complexity than (4.25) and, just as in Appendix B, we do not expect qualitative improvements in the behaviour of the bounds with  $R$ .

The constant  $U$  can be eliminated from (4.25) by following the same procedure outlined in §4.3 in order to obtain a minimization problem that is more suitable for analysis, but less convenient for computations. Indeed, the normalization condition (4.23) implies that the functional  $\mathcal{S}_0\{\hat{T}_0\}$  is minimised when

$$\hat{T}'_0(z) = \frac{\psi'(z) - q(z)}{2b} - \frac{z}{2} + \frac{1}{4} \quad (4.26)$$

and the best  $U$  for given  $a, b, \psi(z)$  and  $q(z)$  is

$$U^* = \frac{1}{2} + \frac{1}{4b} \left\| bz - \frac{b}{2} - \psi'(z) + q(z) \right\|_2^2 - \int_0^1 \psi dz. \quad (4.27)$$

As one would expect, this expression reduces to (4.17) when  $q(z) = -1$ . It is also possible to show that, since we are only interested in nonnegative  $\hat{T}_0$ , the conditions  $\psi(0) = 1$  and  $\psi(1) = 0$  in §4.3 may be weakened into inequalities  $\psi(0) \leq 1$  and  $\psi(1) \leq 0$ . Thus, when the minimum principle for the temperature is imposed, the optimisation problem (4.18) relaxes into

$$\begin{aligned} & \inf_{\psi(z), q(z), a, b} \frac{1}{2} + \frac{1}{4b} \left\| bz - \frac{b}{2} - \psi'(z) + q(z) \right\|_2^2 - \int_0^1 \psi dz \\ \text{subject to } & \psi(0) \leq 1, \psi(1) \leq 0, \quad (4.28) \\ & q(z) \text{ nondecreasing, (4.23),} \\ & \tilde{\mathcal{S}}\{\hat{w}, \hat{T}\} \geq 0 \quad \forall \hat{w}, \hat{T} : (4.8a, b). \end{aligned}$$

Finally, observe that setting  $\psi(z) = 0, q(z) = 0, a = 0$  and letting  $b \rightarrow 0$  in this minimisation problem yields a sequence of feasible solutions with optimal cost approaching  $1/2$  from above irrespective of  $R$ . Thus, the uniform bound  $\langle wT \rangle \leq 1/2$  proved by Goluskin & Spiegel (2012) can be recovered within our approach by taking the auxiliary functional in (4.4) to be

$$\mathcal{V}\{u, T\} = \int_{\Omega} (1 - z)T dx, \quad (4.29)$$

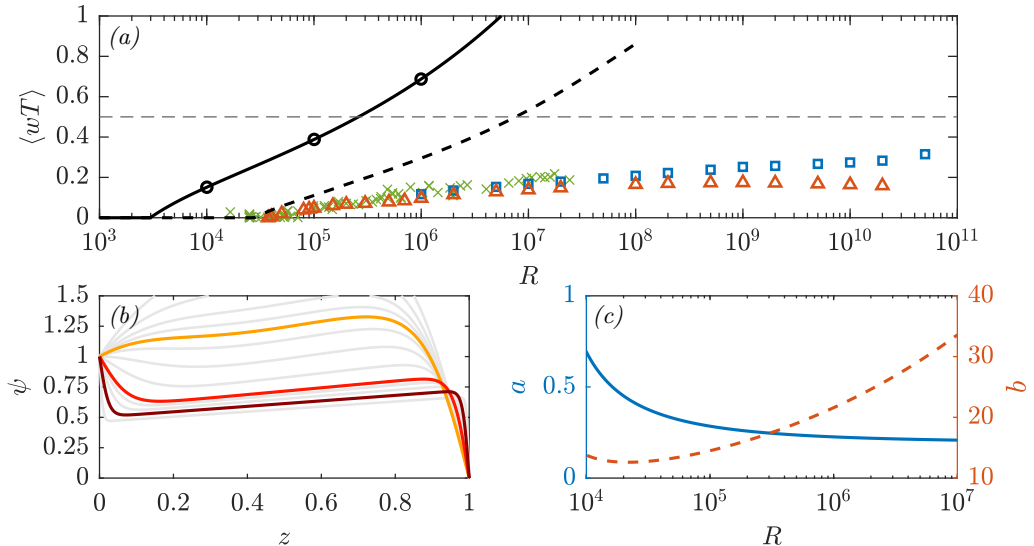


FIGURE 2. (a) Optimal bounds on  $\langle wT \rangle$  obtained by solving the wavenumber-dependent problem (4.12) with horizontal periods  $L_x = L_y = 2$  (•••) and the simplified problem (4.14) (—). Also plotted are experiments by Kulacki & Goldstein (1972) (×), 2D DNSs by Goluskin & Spiegel (2012) (Δ) and 3D DNSs by Goluskin & van der Poel (2016) (◻). Circles mark values of  $R$  at which optimal profiles  $\psi(z)$  are plotted in panel (b). The dashed horizontal line (•••) is the uniform bound  $\langle wT \rangle \leq 1/2$ . (b) Optimal profiles  $\psi(z)$  at  $R = 10^4$  (—),  $10^5$  (—) and  $10^6$  (—). (c) Optimal balance parameters  $a$  (—, left axis) and  $b$  (---, right axis) as a function of  $R$ .

which corresponds to the flow’s potential energy measured with respect to the upper boundary. As shown in §6, however, more general choices can yield better bounds.

## 5. Optimal bounds for general temperature fields

The best upper bounds on  $\langle wT \rangle$  implied by problem (4.12) can be approximated numerically at any fixed Rayleigh number either by deriving and solving the corresponding nonlinear Euler–Lagrange equations (Plasting & Kerswell 2003; Wen *et al.* 2013, 2015), or by discretising it into a semidefinite programme (SDP) (Fantuzzi & Wynn 2015, 2016; Tilgner 2017, 2019; Fantuzzi *et al.* 2018). Here, we choose the latter approach because it preserves the linearity of (4.12); details of our numerical implementation are summarised in Appendix D. Numerically optimal solutions to (4.12) for  $10^3 \leq R \leq 10^7$  are presented in §5.1, while suboptimal but analytical bounds are proved in §5.2.

### 5.1. Numerically optimal bounds

Figure 2 compares the numerically optimal upper bounds  $U$  on the mean vertical heat transfer  $\langle wT \rangle$  to the experimental data by Kulacki & Goldstein (1972) and the DNS data by Goluskin & Spiegel (2012) and Goluskin & van der Poel (2016). The bounds were calculated by solving the minimization problem (4.12) for a fluid layer with horizontal periods  $L_x = L_y = 2$ , and with the simplified problem (4.14), which is independent of wavenectors and, therefore, of  $L_x$  and  $L_y$ . As expected, the bounds obtained with (4.12) are zero when the Rayleigh number is smaller than the energy stability limit  $R_E \approx 29\,723$ , which differs slightly from the value 26 927 reported by Goluskin (2016) due to our

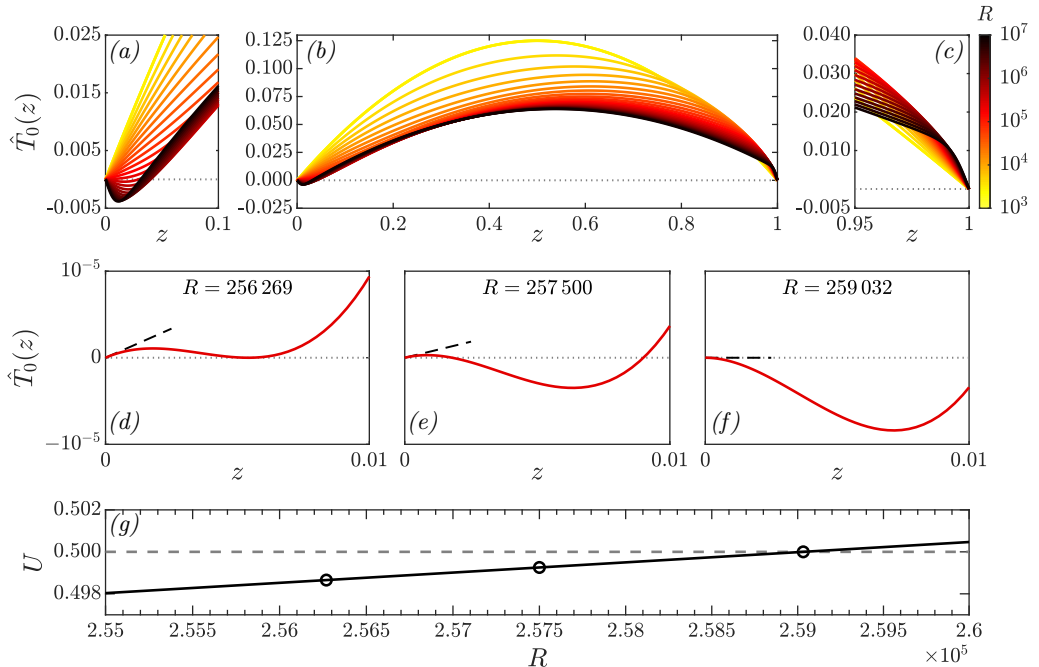


FIGURE 3. *Top*: Critical temperature  $\hat{T}_0(z)$  recovered using (4.16). Colors indicate the Rayleigh number. Panels (a) and (c) show details of the boundary layers. *Middle*: Detailed view of  $\hat{T}_0$  for  $R = 256\,269$ ,  $257\,500$ , and  $259\,032$ . Dashed lines (---) are tangent to  $\hat{T}_0$  at  $z = 0$ . In (d),  $\hat{T}_0$  is nonnegative and has minimum of zero inside the layer. In (e),  $\hat{T}_0$  is initially positive but has a negative minimum. In (f),  $\hat{T}_0'(0) = 0$  and there is no positive initial layer. *Bottom*: Upper bounds  $U$  on  $\langle wT \rangle$ . Circles mark the values of  $R$  considered in (d-f) and  $U = 1/2$  at  $R = 259\,032$ .

choice of horizontal periods. They then increase monotonically with  $R$ , showing the same qualitative behaviour as the bounds computed with the simplified problem (4.14), which reach the value of  $1/2$  at  $R = 259\,032$ . Both sets of results exceed the the uniform upper bound  $\langle wT \rangle \leq 1/2$  for sufficiently large Rayleigh numbers. The apparent contradiction is due to the fact that the uniform bound relies on the minimum principle for the temperature, which was disregarded in the formulation (4.12).

Numerically optimal profiles of  $\psi(z)$  for the simplified bounding problem (4.14) at selected Rayleigh numbers and the variation of the optimal balance parameters  $a$  and  $b$  with  $R$  are illustrated in Figures 2(b) and 2(c) respectively. As expected from the structure of the indefinite term  $(a - \psi')\hat{w}\hat{T}$  of the functional  $\tilde{\mathcal{S}}$ , the derivative  $\psi'$  in the bulk of the domain approaches the value of  $a$  as  $R$  is raised and leads to the formation of two boundary layers. Moreover, the asymmetry of the boundary layers reflects qualitatively the asymmetry of the IH convection problem we are studying, which is characterized by a stable thermal stratification near the bottom boundary ( $z = 0$ ) and an unstable one near the top ( $z = 1$ ). However, note that while  $\psi$  is related to the background temperature field, it is not a physical quantity and need not behave nor scale like the mean temperature in turbulent convection.

Other insightful observations can be made by considering the critical temperature fields  $\hat{T}_0$ , which minimize the functional  $\mathcal{S}_0\{\hat{T}_0\}$  for the optimal choice of  $\psi$ ,  $a$ ,  $b$  and  $U$ . These critical temperatures can be recovered upon integrating (4.16), and are plotted in Figure 3 for a selection of Rayleigh numbers. As one might expect, when  $R$  is sufficiently

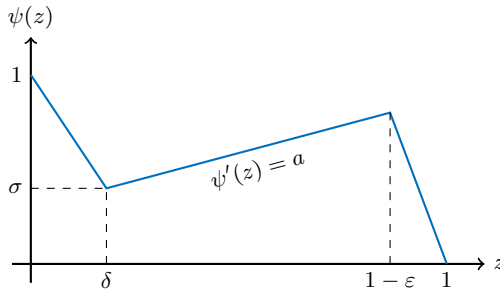


FIGURE 4. General piecewise-linear  $\psi(z)$ , parametrized by the boundary layer widths  $\delta$  and  $\varepsilon$ , the bulk slope  $a$  and the boundary layer height  $\sigma$ . In our proof, we set  $\varepsilon = \delta$  and  $\sigma = \frac{1}{2} - a(\frac{1}{2} - \delta)$  to obtain a profile that is anti-symmetric with respect to  $z = 1/2$ .

small such that  $U = 0$ ,  $\hat{T}_0 = \frac{1}{2}z(1-z)$  coincides with the conductive temperature profile. With the onset of convection and increasing  $R$ , boundary layers form at  $z = 0$  and  $z = 1$  and the maximum of  $|\hat{T}_0|$  decreases. The profiles are also consistent with the uniform rigorous bound  $\langle T \rangle \leq 1/12$  (Goluskin 2016). However, for sufficiently high Rayleigh numbers they are evidently not related to the horizontal and infinite-time averages of the physical temperature field, because they become negative near  $z = 0$ . Interestingly, as shown in Figure 3(d)&(e), this unphysical behaviour first occurs away from the boundary at  $R = 256\,269$ , while the numerical upper bound on  $\langle wT \rangle$  reaches the value of  $1/2$  only at  $259\,032$ , when  $\hat{T}'_0(0) = 0$ . The latter is not surprising because the identity  $\overline{T}'(0) = 1/2 - \langle wT \rangle$ , derived from (1.1) upon recognizing that  $\mathcal{F}_0 = \overline{T}'(0)$ , implies that an upper bound of  $1/2$  on  $\langle wT \rangle$  is equivalent to a zero lower bound on  $\overline{T}'(0)$ , which is obtained when  $\hat{T}'_0(0)$  vanishes. It is therefore clear that the bounding problems (4.12) and (4.14) fail to improve the uniform bound  $\langle wT \rangle \leq 1/2$  proved by Goluskin & Spiegel (2012) at large  $R$  due to a violation of the minimum principle for the temperature, which was not taken into account when formulating them.

### 5.2. A new Rayleigh-dependent analytical bound

The numerical results in the previous section demonstrate that optimising  $\psi$ ,  $a$  and  $b$  cannot improve the uniform bound  $\langle wT \rangle \leq \frac{1}{2}$  at arbitrarily large  $R$ . Nevertheless, it is possible to derive better bounds analytically over a finite range of Rayleigh numbers by considering piecewise-linear profiles  $\psi(z)$  with two boundary layers, such as the one sketched in Figure 4. Even though the numerically optimal profiles in Figure 2 show no symmetry with respect to the vertical midpoint  $z = \frac{1}{2}$ , we impose anti-symmetry and take

$$\psi(z) = \begin{cases} 1 - \left(\frac{a+1}{2\delta} - a\right)z, & 0 \leq z \leq \delta \\ az + \frac{1}{2}(1-a), & \delta \leq z \leq 1-\delta \\ \left(\frac{a+1}{2\delta} - a\right)(1-z), & 1-\delta \leq z \leq 1, \end{cases} \quad (5.1)$$

where  $\delta$  is a boundary layer width to be specified later. This considerably simplifies the algebra, at the cost of a quantitatively (but not qualitatively) worse bound on  $\langle wT \rangle$ . Our goal is to determine values for  $\delta$ ,  $a$  and  $b$  such that  $\psi$  satisfies the constraints in the reduced optimisation problem (4.18), while trying to minimise its objective function.

To show that the functional  $\mathcal{S}_k$  is nonnegative, observe that the only sign-indefinite term in (4.11) is

$$\int_0^1 (a - \psi') \hat{w} \hat{T} dz = \frac{a+1}{2\delta} \int_{[0,\delta] \cup [1-\delta,1]} \hat{w} \hat{T} dz. \quad (5.2)$$

As detailed in Appendix E, this term can be estimated using the fundamental theorem of calculus, the Cauchy–Schwarz inequality, and the boundary conditions (4.8a,b) to conclude that  $\mathcal{S}_k$  is nonnegative if

$$\delta \leq \frac{8\sqrt{2ab}}{(a+1)\sqrt{R}}. \quad (5.3)$$

According to the analysis in §4.3, any choice of  $a$ ,  $b$  and  $\delta$  satisfying this inequality produces the upper bound

$$\begin{aligned} \langle wT \rangle &\leq \frac{1}{2} + \frac{1}{4b} \left\| bz - \frac{b}{2} - \psi'(z) - 1 \right\|_2^2 - \int_0^1 \psi(z) dz \\ &= \frac{b}{48} + \frac{(a+1)^2}{8b\delta} - \frac{(a+1)^2}{4b}. \end{aligned} \quad (5.4)$$

This bound is clearly minimised when  $\delta$  is as large as allowed by (5.3), leading to

$$\langle wT \rangle \leq \frac{b}{48} + \frac{(a+1)^3\sqrt{R}}{64b\sqrt{2ab}} - \frac{(a+1)^2}{4b}. \quad (5.5)$$

The values of  $a$  and  $b$  minimising the right-hand side of this inequality satisfy

$$-\sqrt{b} + \frac{\sqrt{R}}{64\sqrt{2a^3}}(a+1)(5a-1) = 0, \quad (5.6a)$$

$$1 + \frac{12(a+1)^2}{b^2} - \frac{9(a+1)^2\sqrt{R}}{8\sqrt{2ab^5}} = 0, \quad (5.6b)$$

and can be computed numerically for fixed  $R$  to obtain upper bounds plotted as a blue dot-dashed line in Figure 5.

Fully analytical bounds can instead be obtained if we drop the last term from (5.5). In this case, the optimal  $a$  and  $b$  are found explicitly as

$$a = \frac{1}{5} \quad \text{and} \quad b = \frac{9}{5} \left( \frac{R}{2} \right)^{\frac{1}{5}} \quad (5.7)$$

such that we obtain

$$\langle wT \rangle \leq 2^{-\frac{21}{5}} R^{\frac{1}{5}}. \quad (5.8)$$

This bound, plotted as a solid line in Figure 5, is smaller than the uniform bound of  $1/2$  up to  $R = 2^{16} = 65\,536$ , which is approximately 2.43 times larger than the energy stability threshold.

## 6. Optimal bounds for nonnegative temperature fields

The analysis and computations in §5 demonstrate that, if one wants to improve on the uniform bound  $\langle wT \rangle \leq 1/2$  at very large  $R$ , one must invoke the minimum principle for the temperature explicitly to avoid unphysical critical temperatures  $\hat{T}_0$  that are negative in the interior of the layer. As discussed in §4.4, upper bounds on  $\langle wT \rangle$  that take this constraint into account can be found by solving (4.25). Numerically optimal solutions



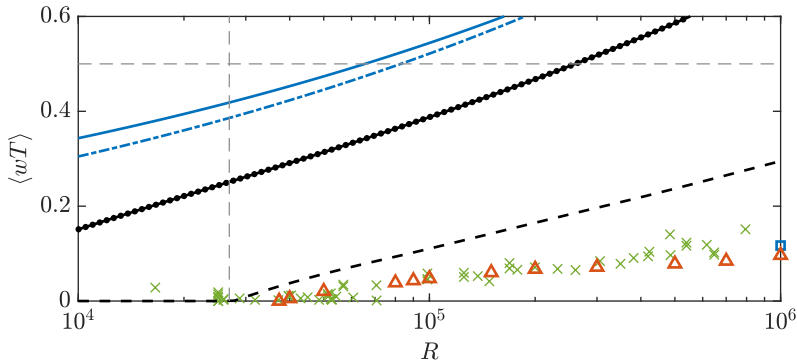


FIGURE 5. Comparison between the semi-analytical bounds computed with (5.5) and (5.6 $_{a,b}$ ) (---), the explicit bound (5.8) (—), the numerically optimal bounds obtained in §5.1 with (4.12) (—,  $L_x = L_y = 2$ ) and with (4.14) (•), and experimental and DNS data (see Figure 2 for a key of the symbols). A dashed vertical line (---) indicates the smallest energy stability threshold,  $R \approx 26\,926$ , while a dashed horizontal line (---) indicates the uniform upper bound  $\langle wT \rangle \leq \frac{1}{2}$ .

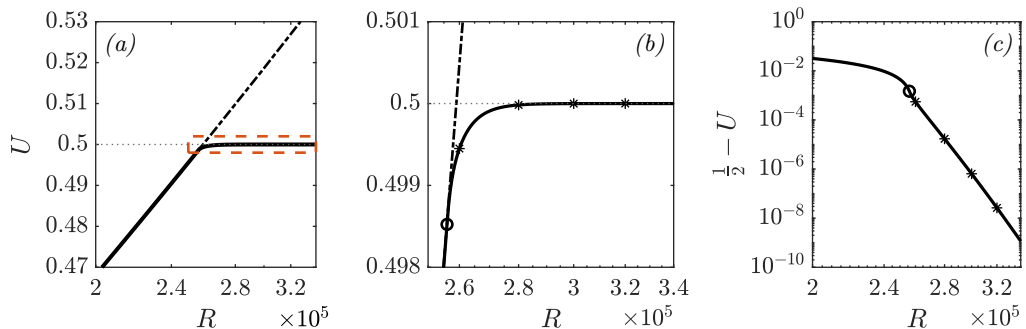


FIGURE 6. (a) Optimal bounds  $U$  on  $\langle wT \rangle$  computed by solving (4.25), which incorporates the minimum principle for temperature (—). Also plotted (---) are the bounds computed in §5 without the minimum principle ( $q(z) = -1$ ). (b) Detail of the region inside the red dashed box (---) in panel (a). (c) Difference between our optimal bounds and the uniform bound  $\langle wT \rangle \leq 1/2$ , shown in all panels as a dotted line (.....). In (b) and (c), a circle at  $R \approx 256\,269$  marks the point at which  $q(z)$  begins to vary from  $-1$ , while stars (\*) mark the Rayleigh numbers at which  $\psi$  are plotted in Figure 7.

to (4.25) are presented in §6.1. Subsection 6.2, instead, gives general conditions under which analytical constructions that attempt to make our numerical results rigorous are guaranteed to fail.

### 6.1. Numerically optimal bounds

Problem (4.25) was discretised into an SDP and solved with the high-precision solver SDPA-GMP (Yamashita *et al.* 2012) for  $2.0 \times 10^5 \leq R \leq 3.4 \times 10^5$ . The MATLAB toolbox SPARSECOLO (Fujisawa *et al.* 2009) was used to exploit sparsity in the SDPs. At each Rayleigh number, we employed the finite-element discretisation approach described in Appendix D on a Chebyshev mesh with at least 6000 piecewise-linear elements, increasing the resolution until the upper bounds changed by less than 1%. Achieving this at  $R = 3.4 \times 10^5$  required approximately 12 200 elements. The numerical challenges associated with setting up the SDPs accurately in double-precision using SPARSECOLO on even finer meshes prevented us from considering a wider the range of Rayleigh numbers.

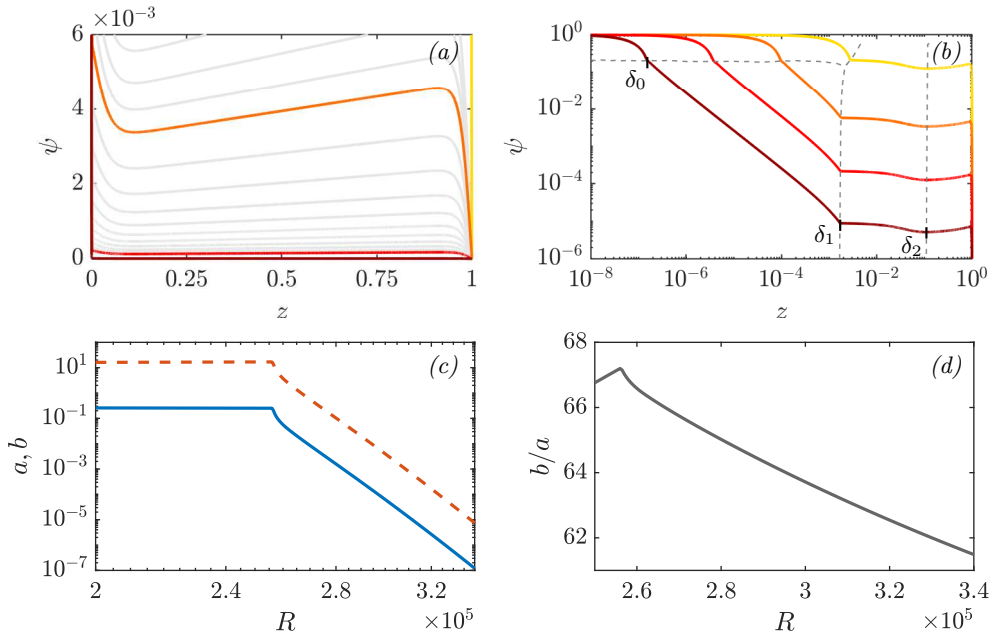


FIGURE 7. (a) Optimal  $\psi(z)$  in the entire domain, plotted for  $0 \leq \psi \leq 0.006$  for visualization purposes. At all  $R$  values,  $\psi(0) = 1$ . (b) Logarithmic plot of  $\psi(z)$ , highlighting the behaviour near  $z = 0$ . Coloured lines correspond to the  $R$  highlighted in Figure 6, for  $R = 2.6 \times 10^5$  (—),  $2.8 \times 10^5$  (—),  $3.0 \times 10^5$  (—),  $3.2 \times 10^5$  (—). Dashed lines (---) mark the boundaries of the sublayers  $(0, \delta_0)$ ,  $(\delta_0, \delta_1)$  and  $(\delta_1, \delta_2)$ , and the sublayer edges are labelled explicitly for  $R = 3.2 \times 10^5$ . (c) Variation with  $R$  of the optimal balance parameters  $a$  (—) and  $b$  (---) for (4.25). (d) Ratio of balance parameters,  $b/a$ , when the Lagrange multiplier is active.

Figure 6 compares numerical upper bounds on the heat transfer obtained with (solid line) and without (dot-dashed line) the minimum principle for the temperature, that is, by optimising  $q(z)$  or by setting  $q(z) = -1$  in (4.25), respectively. The results for the latter case coincide with those described in §5.1 and shown in Figure 2.

The choice  $q(z) = -1$  is optimal for  $R < 256\,269$ . For higher  $R$ , the numerical upper bounds on  $\langle wT \rangle$  with optimised  $q(z)$  are strictly better than those with  $q(z) = -1$  and, crucially, appear to approach the uniform bound  $\frac{1}{2}$  from below as  $R$  is raised. Note that although the deviation from  $\frac{1}{2}$  is small at the highest values of  $R$  that could be handled, it is much larger than the tolerance ( $10^{-25}$ ) used by the multiple-precision SDP solver SDPA-GMP, giving us confidence that it is not a numerical artefact. Moreover, the deviation from  $\frac{1}{2}$  of the numerical bounds, shown in Figure 6(c), appears to decay as a power law, suggesting that the optimal bound available within our bounding framework may have the functional form (1.2). Although the range of Rayleigh numbers spanned by our computations is too small to accurately predict the exponent and the prefactor, it is clear that the decay is much faster than predicted by the heuristic arguments in §3.

Optimal profiles  $\psi(z)$  for selected Rayleigh numbers are shown in Figures 7(a,b) and differ significantly from the corresponding profiles in Figure 2(b) obtained when the minimum principle for the temperature is disregarded. When the minimum principle is enforced,  $\psi$  appears to approach zero almost everywhere as  $R$  is raised, but always satisfies  $\psi(0) = 1$ . This leads to the formation of a very thin boundary layer near  $z = 0$ , which at high  $R$  consists of three distinct sublayers identified by two points,  $z = \delta_0$  and  $z = \delta_1$ , at which  $\psi$  is not differentiable. These are indicated by gray dashed lines in

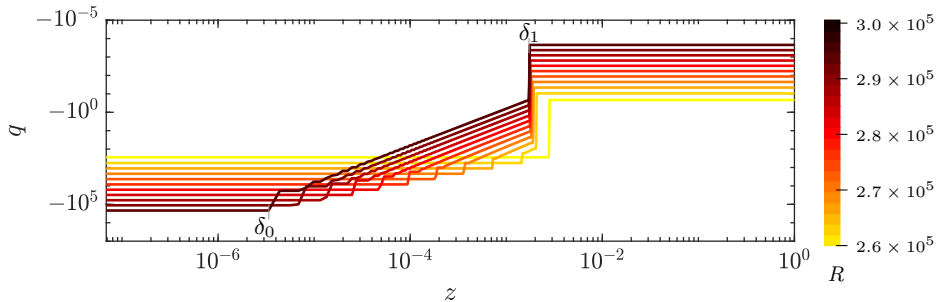


FIGURE 8. Variation of  $q(z)$  shown on a logarithmic scale to highlight the non-zero region of the Lagrange multiplier  $q'(z)$ , from  $R = 2.6 - 3.0 \times 10^5$ . The colorbar here applies for all  $\psi$ ,  $q$  and  $\hat{T}_0$  presented in §6. The edges of the boundary sublayers  $(0, \delta_0)$  and  $(\delta_0, \delta_1)$  for the largest  $R$  value are explicitly labelled.

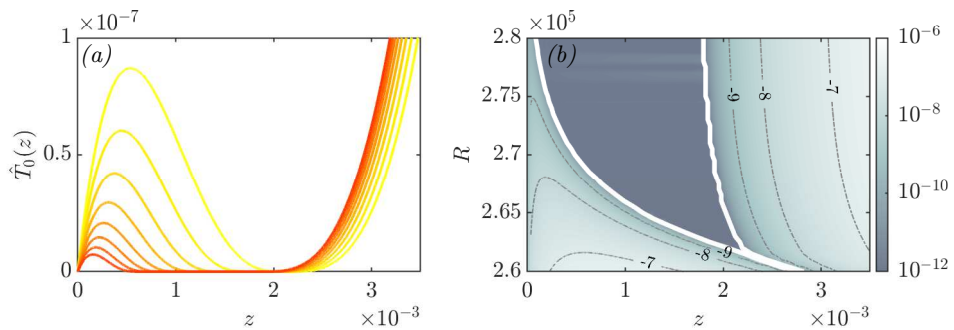


FIGURE 9. Variation with  $R$  of the critical temperature profiles,  $\hat{T}_0$ , plotted for  $0 \leq z \leq 3.5 \times 10^{-3}$ . (a) Plots of individual  $\hat{T}_0$  from  $R = 2.62 - 2.69 \times 10^5$ . (b) Contour plot of  $\hat{T}_0$  vs  $R$ . Solid white lines mark the boundary sublayer  $\delta_0 \leq z \leq \delta_1$ , within which  $q' > 0$  and  $\hat{T}_0 = 0$ . Values of  $\hat{T}_0$  below  $10^{-12}$  are assumed to be numerical zeros.

Figure 7(b). In the first sublayer, from  $z = 0$  to  $z = \delta_1$ ,  $\psi$  is observed to vary linearly. The second sublayer,  $\delta_0 < z < \delta_1$ , is observed only for  $R > 2.6 \times 10^5$  and we observe that  $\psi \sim z^{-1}$  approximately. The third sublayer, from  $z = \delta_1$  to the point  $z = \delta_2$  at which  $\psi$  attains a local minimum, does not have a simple functional form. In the bulk,  $\psi$  increases approximately linearly with slope very close to  $a$ , as was the case in §5, and the condition  $\psi(1) = 0$ , which emerges as a result of the optimization and is not imposed *a priori*, is attained through a small boundary layer of width  $\varepsilon$  near  $z = 1$ . We choose the boundary of this layer as the point  $z = 1 - \varepsilon$  at which  $\psi$  has a local maximum.

Figure 7(c) shows the variation of the balance parameters with  $R$ . Below 256 269, both coincide with the values plotted in Figure 2(c). At higher  $R$ , the minimum principle for the temperature becomes active and both balance parameters start to decay rapidly. It would be tempting to conjecture that  $a \sim b \sim R^{-p}$  for some power  $p$  but, given the small variation of  $b/a$  evident in Figure 7(d), we cannot currently exclude that subtly different scaling exponents or higher-order corrections do not play an important role in obtaining an upper bound on  $\langle wT \rangle$  that approaches  $\frac{1}{2}$  asymptotically from below.

Figure 8 shows the structure of  $q$ , whose (distributional) derivative represents the Lagrange multiplier enforcing the minimum principle. The multiplier, therefore, is active in regions where  $q$  is not constant. The choice  $q(z) = -1$  is optimal for  $R = 256\,269$ . At higher Rayleigh numbers, the multiplier becomes active between  $z = \delta_0$  and  $z = \delta_1$ ,

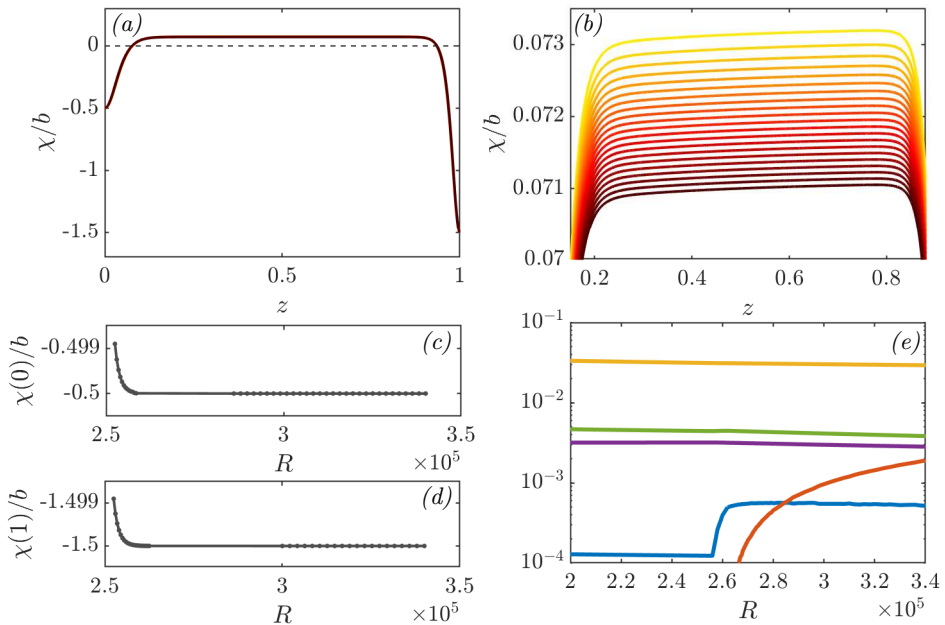


FIGURE 10. (a) Profiles  $\chi(z)/b$  for  $2.6 \times 10^5 \leq R \leq 3.0 \times 10^5$ . (b) Detailed view of  $\chi(z)/b$  in the bulk. (c,d) Variation of  $\chi(0)/b$  and  $\chi(1)/b$  with  $R$ . (e) Contributions to the integral of  $\psi/b$  in the regions  $(0, \delta_0)$  (—),  $(\delta_0, \delta_1)$  (—),  $(\delta_1, \delta_2)$  (—),  $(\delta_2, 1 - \varepsilon)$  (—) and  $(1 - \varepsilon, 1)$  (—), as a function of  $R$ .

which is what causes the second boundary sublayer in  $\psi$ . In the immediate vicinity of the bottom boundary ( $0 \leq z \leq \delta_0$ ),  $q$  is constant and it appears that  $q(z) - \psi'(z) \approx b/2$  (cf. Figure 10(c)). Indeed, inspection of the cost function in (4.28) suggests that  $q(z) - \psi'(z) = b(1 - z)/2$  should be optimal, but we could not identify the very small  $z$ -dependent correction in our numerical results. In the second sublayer ( $\delta_0 \leq z \leq \delta_1$ ), where the Lagrange multiplier is active,  $q(z) \sim -z^{-2}$ . Again, this is consistent with the minimization of the cost function in (4.28), as one expects  $q$  to cancel the very large contribution of  $\psi'$  near the bottom boundary.

Further validation of our numerical results comes from inspection of the critical temperatures  $\hat{T}_0(z)$ , which can be recovered using (4.26) and are shown in Figure 9(a,b) for selected values of  $R$ . As expected, the critical temperatures are nonnegative for all  $z$  and vanish identically (up to small numerical tolerances) in the region  $\delta_0 \leq z \leq \delta_1$ , where  $q$  is active. We note that, for a given Rayleigh number, this region is strictly larger than the range of  $z$  values for which the critical temperatures in Figure 3(c) are negative, indicating that the minimum principle alters the problem in a more subtle way than simply saturating the constraint  $T \geq 0$ .

To analyse the results further we define the diagnostic function

$$\chi(z) = \psi'(z) - q(z), \quad (6.1)$$

and rewrite (4.27) as

$$\langle wT \rangle \leq \frac{1}{2} + b \left[ \int_0^1 \frac{1}{4} \left( z - \frac{1}{2} - \frac{\chi(z)}{b} \right)^2 - \frac{\psi(z)}{b} dz \right]. \quad (6.2)$$

Panels (a), (c) & (d) in Figure 10 suggest that  $\chi(0)/b \rightarrow -\frac{1}{2}$  and  $\chi(1)/b \rightarrow -\frac{3}{2}$  as  $R \rightarrow \infty$ . In fact, profiles  $\chi(z)/b$  for different Rayleigh numbers collapse almost exactly throughout the layer, but subtle corrections are present; for instance, Figure 10(b) demonstrates that, in the bulk, the mean value of  $\chi(z)/b$  decreases with  $R$ . It is also evident that  $\chi(z)$  is not exactly constant throughout the bulk, but increases by approximately  $10^{-4}$ . Since  $q(z)$  is constant in this region, we conclude that  $\psi'(z)$  is not constant, but displays subtle and thus nontrivial variation.

Figure 10(e) illustrates the variation with  $R$  of contributions to the integral of  $\psi(z)/b$  from regions  $(0, \delta_0)$ ,  $(\delta_0, \delta_1)$ ,  $(\delta_1, \delta_2)$ ,  $(\delta_2, 1 - \varepsilon)$  and  $(1 - \varepsilon, 1)$ . The largest contribution comes from the bulk ( $\delta_2 \leq z \leq 1 - \varepsilon$ ), but it slowly decreases with  $R$ . The same is true of the contribution of the top boundary layer ( $1 - \varepsilon \leq z \leq 1$ ) and the outermost boundary sublayer near  $z = 0$  ( $\delta_1 \leq z \leq \delta_2$ ). Only in the first two boundary layers near  $z = 0$  does the value of the integral increase with  $R$ , suggesting that the integral of  $\psi(z)/b$  near the boundary layer may become the dominant term as  $R \rightarrow \infty$ . While the range of Rayleigh numbers covered by our computations is too small to confirm or disprove this conjecture, it is certain that the integral of  $\psi(z)/b$  must remain large enough to offset the positive term in (6.2) in order to obtain a bound on  $\langle wT \rangle$  smaller than  $1/2$ .

Finally, Figures 8 and 10 suggest that, for sufficiently large  $R$ ,

$$q(z) = \begin{cases} \psi'(z) + \frac{b}{2}, & 0 \leq z \leq \delta_0, \\ -q_0 z^{-2}, & \delta_0 \leq z \leq \delta_1, \\ \psi'(1) + \frac{3b}{2}, & \delta_1 \leq z \leq 1, \end{cases} \quad (6.3)$$

for some positive constant  $q_0$ , and that  $a, \psi, q_0 \sim b$ . The next section investigates whether such ansatz can lead to upper bounds on  $\langle wT \rangle$  that are strictly smaller than  $1/2$  at all Rayleigh numbers.

## 6.2. Towards an analytical bound

The numerical evidence presented in §6.1 suggests that the upper bound on  $\langle wT \rangle$  obtained from the optimization problem (4.28) approaches  $\frac{1}{2}$  asymptotically from below as  $R \rightarrow \infty$ . To confirm this observation with a proof requires, for every  $R \geq 1$ , construction of feasible decision variables  $a, b, \psi(z), q(z)$  whose corresponding cost is strictly less than  $\frac{1}{2}$ . This section discusses the challenges presented by this goal. Specifically, we show that no construction is possible if one tries to mimic key properties of the numerically optimal decision variables presented in §6.1 and, at the same time, enforces the spectral constraint using estimates typically used in successful applications of the background method.

To aid the discussion, the following definition introduces three subsets  $\mathcal{A}, \mathcal{B}$  and  $\mathcal{C}$  of decision variables that capture some of the properties observed from our numerical study.

**DEFINITION 1.** *Let  $0 < \delta < 1 - \varepsilon < 1$  and  $\gamma > 0$  and  $R \geq 1$ . Decision variables  $(a, b, \psi(z), q(z))$  are said to belong to:*

1. *The set  $\mathcal{A}\{\delta, \varepsilon\}$  if the following conditions hold:*
  - (a) *The balance parameters satisfy  $0 < a \leq b$ ;*
  - (b)  *$\psi \in C^1[0, 1]$  with boundary conditions  $0 \leq \psi(0) \leq 1$  and  $\psi(1) = 0$ ;*
  - (c) *The derivative of  $\psi$  satisfies  $\psi'|_{[0, \delta]} \leq 0$ ,  $\psi'|_{[\delta, 1 - \varepsilon]} \geq 0$ , and  $\|\psi'\|_{L^\infty(1 - \varepsilon, 1)} \leq 2b$ .*
2. *The set  $\mathcal{B}\{\gamma\}$  if both  $\psi'(z)$  and  $q(z)$  are constant on the interval  $(\frac{1}{2} - \gamma, \frac{1}{2} + \gamma)$ .*
3. *The set  $\mathcal{C}\{\delta, \varepsilon, R\}$  if*

$$\delta^2 \|a - \psi'\|_{L^\infty(0, \delta)} + \varepsilon^2 \|a - \psi'\|_{L^\infty(1 - \varepsilon, 1)} \leq 8\sqrt{\frac{2ab}{R}}.$$

The set  $\mathcal{A}\{\delta, \varepsilon\}$  contains profiles  $\psi$  which possess an initial (and potentially severe) boundary layer in an interval  $[0, \delta]$ , then increase in a bulk region  $[\delta, 1 - \varepsilon]$ , before approaching  $\psi(1) = 0$  in an upper boundary layer contained in the interval  $[1 - \varepsilon, 1]$  and in which  $\psi'$  is controlled by the balance parameter  $b$ , as seen in previous results. Optimal decision variables  $(a, b, \psi(z), q(z))$  obtained in §6.1 appear, with compelling evidence, to belong to a set of the form  $\mathcal{A}\{\delta, \varepsilon\}$  with the exception of the differentiability condition  $\psi \in C^1[0, 1]$ . Indeed, the optimal profiles  $\psi$  appear to be piecewise differentiable, losing differentiability at two points corresponding to the boundaries of non-constant behaviour of the multiplier  $q(z)$  observed in figure 8. However, since no higher derivatives of  $\psi$  appear in the optimization problem (4.28), adding the constraint  $(a, b, \psi(z), q(z)) \in \mathcal{A}$  to (4.28) will not change its optimal cost.

The set  $\mathcal{B}\{\gamma\}$  contains decision variables for which  $\psi'$  and  $q$  are constant in some interval centred at  $\frac{1}{2}$ . Figures 8 and 10 reveal that this is not the case for the numerically optimal  $\psi$ , so the use of  $\mathcal{B}\{\gamma\}$  corresponds to a proof which ignores subtle variations from a purely linear profile away from the boundaries. Without further assumptions (say, restriction to fluids with infinite Prandtl number), it is not clear how such variations can be exploited in analytical constructions.

The set  $\mathcal{C}\{\delta, \varepsilon, R\}$  relates to a choice of profiles  $\psi$  and balance parameters  $a, b$  for which the constraint  $\mathcal{S}_k \geq 0$  can be proven to hold for a given  $R$ . In particular, if  $a, b, \psi(z)$  satisfy (E 11) and it is the case that  $\psi'|_{[\delta, 1-\varepsilon]} = a$ , then the argument in Appendix E implies that  $\tilde{\mathcal{S}} \geq 0$ . Specifically,  $\mathcal{C}\{\delta, \varepsilon, R\}$  provides sufficient control of the severity of the boundary layers of  $\psi$  for the spectral constraint to be provably satisfied. While crude, estimates of this form in conjunction with constant  $\psi'(z)$  in a bulk region  $\delta \leq z \leq 1 - \varepsilon$  are employed for almost all analytical constructions of background fields.

We now return to the original question of attempting to upper-bound  $\langle wT \rangle$  via an analytical construction of feasible decision variables  $(a, b, \psi(z), q(z))$  for (4.28). It is not unreasonable, based upon the above evidence, to propose  $R$ -dependent balance parameters  $a = a_R, b = b_R$ , boundary layer widths  $\delta = \delta_R, \varepsilon = \varepsilon_R$  and profiles  $\psi_R, q_R$  which satisfy

$$(a_R, b_R, \psi_R(z), q_R(z)) \in \mathcal{A}\{\delta_R, \varepsilon_R\} \cap \mathcal{B}\{\gamma\} \cap \mathcal{C}\{\delta_R, \varepsilon_R, R\}, \quad R \geq 1,$$

for some  $\gamma > 0$ . The following result shows that, for such a construction, there is a hard lower bound on the optimal cost achievable using (4.28).

**PROPOSITION 1.** *Let  $0 < \delta < 1 - \varepsilon < 1$  and  $\gamma > 0, R \geq 1$ . Suppose that*

$$(a, b, \psi(z), q(z)) \in \mathcal{A}\{\delta, \varepsilon\} \cap \mathcal{B}\{\gamma\} \cap \mathcal{C}\{\delta, \varepsilon, R\}. \quad (6.4)$$

*Then*

$$\frac{1}{4b} \left\| bz - \frac{b}{2} - \psi'(z) + q(z) \right\|_2^2 - \int_0^1 \psi \, dz \geq \frac{b}{6} \left( \gamma^3 - 24 \cdot \frac{1 + 2\sqrt{2}}{R^{\frac{1}{4}}} \right).$$

From the proof in Appendix F, the consequence of Proposition 1 is the following. If one constructs feasible decision variables for the optimization problem (4.28) which satisfy (6.4), then the best achievable bound  $U$  for which  $\langle wT \rangle \leq U$  must satisfy

$$U \geq \frac{1}{2} + \frac{b}{6} \left( \gamma^3 - 24 \cdot \frac{1 + 2\sqrt{2}}{R^{\frac{1}{4}}} \right).$$

Hence, using such a construction with the assumption that  $\psi'$  and  $q$  are constant in a bulk region  $(\frac{1}{2} - \gamma, \frac{1}{2} + \gamma)$ , it is not possible to prove that  $\langle wT \rangle < \frac{1}{2}$  at arbitrarily high Rayleigh number.

Consequently, one must ask what conditions should be dropped if a rigorous bound  $\langle wT \rangle < \frac{1}{2}, R \geq 1$ , is to be found. The numerical evidence presented in §6.1 suggests that the optimal decision variables do belong to  $\mathcal{A}$ . Consequently, either  $\mathcal{B}$  or  $\mathcal{C}$  must be dropped. Figure 8 indicates that optimal multipliers  $q(z)$  are constant outside a lower boundary layer. Hence, dropping  $\mathcal{B}$  corresponds to choosing a profile with non-constant  $\psi'(z)$  in the bulk; the cost function of (4.28) and Figure 10(b) suggests that a quadratic ansatz for  $\psi(z)$  may be beneficial. Dropping  $\mathcal{C}$  corresponds to requiring more sophisticated analysis of the spectral constraint. Using these insights will be the focus of future research.

## 7. Conclusions

We obtained upper bounds  $U$  on the vertical heat transport  $\langle wT \rangle$  in IH convection that improve on the best existing bound  $\langle wT \rangle \leq 1/2$  (Goluskin & Spiegel 2012). Crucially, we demonstrated that, within our bounding framework, the existing uniform bound can be improved only up to a finite value of the Rayleigh number  $R$  unless non-physical negativity of the optimal temperature field is prevented. Specifically, we constructed an analytical proof that  $\langle wT \rangle \leq 2^{-\frac{24}{5}} R^{1/5}$ , which improves on the uniform bound for  $R < 2^{16} = 65\,536$  (2.43 times larger than the energy stability threshold). However, our numerical results suggest that the best available bound tends to  $1/2$  asymptotically from below as  $R \rightarrow \infty$  when a Lagrange multiplier is introduced to enforce non-negativity of the optimal temperature field.

A numerical challenge encountered in this work was in the implementation of the optimisation problem (4.25). The sharp boundary layers in  $\psi$  and  $q$  near  $z = 0$  require extremely high resolution and, consequently, a fine mesh. This poses challenges not only in terms of computational cost, but also in terms of numerical accuracy. Using a simplification of the spectral constraint we obtained results for a limited range of  $R$ , but in order to shed light on the problems highlighted above, possible improvements to the algorithm or problem's formulation remain a point of interest and opportunity for further research.

As explained in §6.2, the prospect of obtaining an analytical proof that  $U \rightarrow 1/2$  strictly from below as  $R \rightarrow \infty$  requires the use of more sophisticated estimates to satisfy the spectral constraint than those that are typically used. Such improvements are necessary, rather than sufficient, conditions because there is a possibility that  $U = 1/2$  for values of  $R$  that lie outside the range that we have studied numerically. In this regard, the numerical results, which correspond to the best available bound for quadratic auxiliary functions, suggest either exponential or extremely strong algebraic scaling of  $U$  towards  $1/2$  in  $R$  that is far from any of the heuristic scaling possibilities discussed in §3. More sophisticated treatments of the spectral constraint might yield a proof that  $U \rightarrow 1/2$  strictly from below, but they are unlikely to prove bounds that correspond to heuristic scaling arguments. Either IH convection defies all of the heuristics invoked in §3 or the quadratic auxiliary function framework is unable to access a crucial aspect of the system's properties. The latter could be explored further by investigating a larger class of auxiliary functions (Goluskin & Fantuzzi 2019; Fantuzzi *et al.* 2016; Chernyshenko *et al.* 2014), but at the possible expense of analytical or even numerical tractability.

**Acknowledgements** We are grateful to D. Goluskin for enlightening us on many aspects of IH convection and for sharing his DNS data. This work also benefited from conver-



sations with C. Nobili, J. Whitehead, C. R. Doering, I. Tobasco and G. O. Hughes. AA acknowledges funding by the EPSRC Centre for Doctoral Training in Fluid Dynamics across Scales (award number EP/L016230/1). GF gratefully acknowledges the support of an Imperial College Research Fellowship and the hospitality of the 2018 GFD program at Woods Hole Oceanographic Institution, where this work was begun.

**Conflict of interests** The authors report no conflict of interests.

## Appendix A. Minimum principle in IH convection

A minimum principle for IH convection can be proved by adapting arguments for Rayleigh–Bénard convection (Foias *et al.* 1987, Lemma 2.1). Let

$$T_-(\mathbf{x}, t) := \max\{-T(\mathbf{x}, t), 0\} \quad (\text{A } 1)$$

denote the negative part of  $T$  and observe that  $T_-$  is nonnegative on the fluid’s domain  $\Omega$ . Multiplying the advection-diffusion equation (2.1c) by  $T_-$  and integrating by parts over the domain using the boundary conditions and incompressibility yields

$$\frac{1}{2} \frac{d}{dt} \|T_-\|_2^2 = -\|\nabla T_-\|_2^2 - \int_{\Omega} T_- \, d\mathbf{x}. \quad (\text{A } 2)$$

Upon observing that the last integral on the right-hand side is positive and that  $T_-$  vanishes at the top and bottom boundaries, so  $\|\nabla T_-\|_2^2 \geq \mu \|T_-\|_2^2$  for some constant  $\mu > 0$  by the Poincaré inequality, we can estimate

$$\frac{1}{2} \frac{d}{dt} \|T_-\|_2^2 \leq -\mu \|T_-\|_2^2. \quad (\text{A } 3)$$

Gronwall’s lemma then yields

$$\|T_-(t)\|_2^2 \leq \|T_-(0)\|_2^2 e^{-\mu t}, \quad (\text{A } 4)$$

so  $T_-$  tends to zero in  $L^2(\Omega)$  at least exponentially quickly. This implies that  $T(\mathbf{x}, t) \geq 0$  almost everywhere on the global attractor and that  $T(\mathbf{x}, t)$  is nonnegative at all times if it is so at  $t = 0$ .

## Appendix B. Comparing the full and simplified spectral constraints

This appendix provides further computational evidence that replacing the spectral constraints  $\mathcal{S}_{\mathbf{k}} \geq 0$  with the single, stronger constraint  $\tilde{\mathcal{S}} \geq 0$  does not affect the qualitative behaviour of the optimal bounds on  $\langle wT \rangle$ . The simplified optimization problem (4.14) was solved using the finite-element expansion approach described in appendix (D). For simplicity, instead, the wavenumber-dependent problem (4.12) was solved using the general-purpose toolbox QUINOPT (Fantuzzi *et al.* 2017), which implements Legendre series expansions. The critical wavenumbers were determined with the help of the following result.

LEMMA 1. Fix  $R$ ,  $a$ ,  $b$  and  $\psi(z)$  satisfying  $\psi(0) = 1$  and  $\psi(1) = 0$ . The inequality  $\mathcal{S}_{\mathbf{k}}\{\hat{w}_{\mathbf{k}}, \hat{T}_{\mathbf{k}}\} \geq 0$  holds for all  $\hat{w}_{\mathbf{k}}$  and  $\hat{T}_{\mathbf{k}}$  satisfying conditions (4.8a,b) if

$$k^4 \geq \frac{R}{4ab} \|a - \psi'\|_{\infty}^2. \quad (\text{B } 1)$$

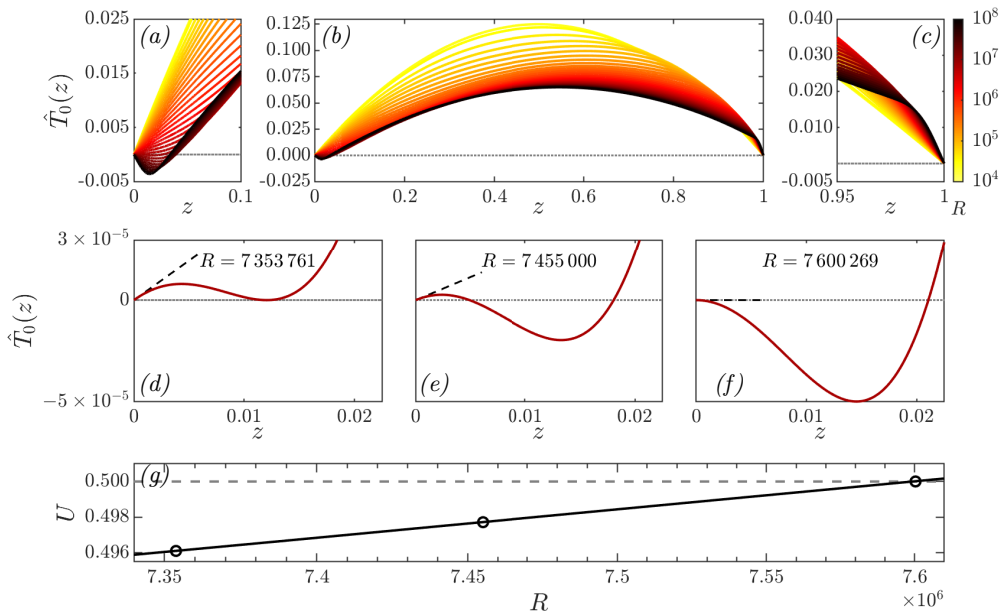


FIGURE 11. *Top*: Critical temperature  $\hat{T}_0(z)$  recovered using (4.16) when the spectral constraint is given by  $\mathcal{S}_{\mathbf{k}} > 0$ . Colors indicate the Rayleigh number. Panels (a) and (c) show details of the boundary layers. *Middle*: Detailed view of  $\hat{T}_0$  for  $R = 7353761$ ,  $7455000$ , and  $7600269$ . Dashed lines (---) are tangent to  $\hat{T}_0$  at  $z = 0$ . In (d),  $\hat{T}_0$  is nonnegative and has minimum of zero inside the layer. In (e),  $\hat{T}_0$  is initially positive but has a negative minimum. In (f),  $\hat{T}_0(0) = 0$  and there is no positive initial layer. *Bottom*: Upper bounds  $U$  on  $\langle wT \rangle$ . Circles mark the values of  $R$  considered in (d-f) and  $U = 1/2$  at  $R = 7600269$ .

*Proof.* The Hölder and Cauchy–Schwarz inequalities yield

$$\left| \int_0^1 (a - \psi') \hat{w}_{\mathbf{k}} \hat{T}_{\mathbf{k}} dz \right| \leq \|a - \psi'\|_{\infty} \|\hat{w}_{\mathbf{k}}\|_2 \|\hat{T}_{\mathbf{k}}\|_2. \quad (\text{B } 2)$$

Consequently,

$$\mathcal{S}_{\mathbf{k}} \geq \frac{ak^2}{R} \|\hat{w}_{\mathbf{k}}\|_2^2 - \|a - \psi'\|_{\infty} \|\hat{w}_{\mathbf{k}}\|_2 \|\hat{T}_{\mathbf{k}}\|_2 + bk^2 \|\hat{T}_{\mathbf{k}}\|_2^2. \quad (\text{B } 3)$$

The right-hand side is a homogeneous quadratic form in  $\|\hat{w}_{\mathbf{k}}\|_2$  and  $\|\hat{T}_{\mathbf{k}}\|_2$  and is nonnegative for any choice of  $\hat{w}_{\mathbf{k}}$  and  $\hat{T}_{\mathbf{k}}$  if and only if (B1) holds.  $\square$

This result guarantees that, when implementing (4.12) numerically, it suffices to consider wavenumbers with

$$k < \left( \frac{R}{4ab} \right)^{\frac{1}{4}} \|a - \psi'\|_{\infty}^{\frac{1}{2}}. \quad (\text{B } 4)$$

While the right-hand side of this inequality is unknown a priori, as it depends on the optimisation variables  $a$ ,  $b$  and  $\psi$ , in practice one can simply solve (4.12) using all wavevectors with  $k$  smaller than an arbitrarily chosen value. Then, one checks whether  $\mathcal{S}_{\mathbf{k}}$  is indeed nonnegative for all  $k$  satisfying (B4), and repeats the computation with

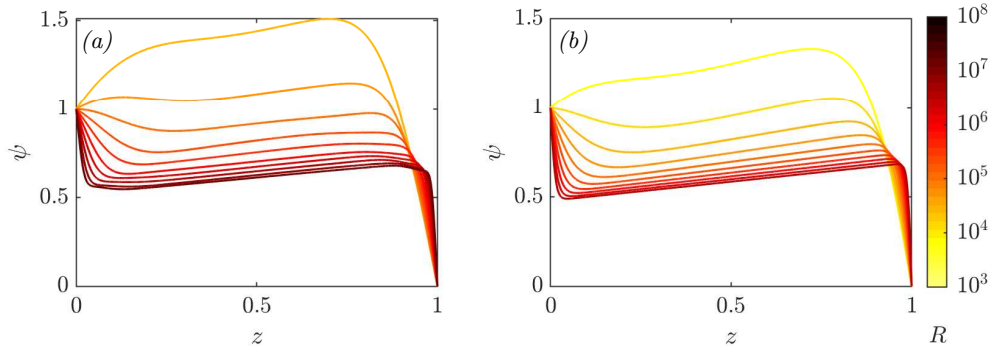


FIGURE 12. (a) Optimal  $\psi(z)$  for selected Rayleigh numbers (see colorbar) obtained by solving optimization problem (4.12), which imposes the exact spectral constraints  $\mathcal{S}_{\mathbf{k}} \geq 0$ . (b) Optimal  $\psi(z)$  at the same Rayleigh numbers but obtained by solving optimization problem (4.14), which imposes the simplified spectral constraint  $\tilde{\mathcal{S}} \geq 0$ .

a larger set of wavevectors if these checks fail. Upper bounds obtained by solving the full problem (4.12) and the simplified problem (4.14) are shown in Figure 2. Here we demonstrate the equivalence of the results for both spectral constraints qualitatively. As expected, using the simplified spectral constraint yields worse bounds at a fixed Rayleigh number. While the full spectral constraint yields bounds that are zero up for all  $R$  up to the energy stability threshold, which depends on the choice of horizontal periods  $L_x$  and  $L_y$ , the simplified functional  $\tilde{\mathcal{S}}$  is insensitive to these values and gives a conservative estimate for the nonlinear stability threshold. Nevertheless, both sets of result display the same qualitative increase as  $R$  is raised. This is further demonstrated in Figures 11, which can be compared to Figure 3

In particular, the upper bound reaches  $1/2$  exactly when the critical temperature  $\hat{T}_0$ , which minimizes the functional  $\mathcal{S}_0$ , has zero gradient at  $z = 0$ , as can be observed in Figures 11(f) & (g). Shown in panels (a)-(c) are the critical temperature fields,  $\hat{T}_0$ , for  $10^4 \leq R \leq 10^8$ . In the middle row of the figure, going from left to right, observe first that for  $R > 7353761$  the critical temperature is negative in the domain. Then panel (e) shows a  $R$  at which  $\hat{T}_0$  is positive in a small region very close to the wall but clearly violates the minimum principle further away. In (f), where  $R = 7600269$ , for our choice of  $L_x = L_y = 2$ , the numerically optimal bound passes the uniform bound, at which point we have  $\hat{T}'_0(0) = 0$ . These results for the  $\mathbf{k}$ -dependent spectral constraint qualitatively match the results for the simplified spectral constraint (4.13) presented Figure 3.

As evidenced by Figure 12, the optimal  $\psi$  obtained with the full and simplified spectral constraints also display similar features. The only notable difference is the non simple behaviour near the boundary layer of the optimal profiles  $\psi$  for the full problem (4.12), which arise after bifurcations in the critical wavenumbers as  $R$  is raised. In panel (b), instead,  $\psi$  exhibits a simple structure in both of the boundary layers.

These observations confirm that strengthening the spectral constraints using the wavevector-independent functional  $\tilde{\mathcal{S}}$  only affects our computational results quantitatively, but preserves the overall qualitative behaviour.

### Appendix C. Justification of (4.21)

To justify the choice of bounded linear functional in (4.21), we start with a technical lemma. In this appendix,  $\mathcal{T}$  is the space of square-integrable temperature fields in the Sobolev space  $H^1(\Omega)$  that are horizontally periodic and vanish at  $z = 0$  and  $1$ . We equip  $\mathcal{T}$  with the inner product  $(T_1, T_2) = \int_{\Omega} \nabla T_1 \cdot \nabla T_2 \, d\mathbf{x}$ .

**LEMMA 2.** *Let  $q : (0, 1) \rightarrow \mathbb{R}$  be a square-integrable function. The bounded linear functional  $\mathcal{L}_q : \mathcal{T} \rightarrow \mathbb{R}$  given by  $\mathcal{L}_q(T) = - \int_{\Omega} q(z) \frac{\partial T}{\partial z} \, d\mathbf{x}$  is positive if and only if  $q(z)$  is nondecreasing.*

*Proof.* First, we prove that  $q$  is nondecreasing if  $\mathcal{L}_q$  is a positive functional. Fix any  $z_1, z_2 \in (0, 1)$  with  $z_1 < z_2$  and choose  $\varepsilon > 0$  small enough that  $0 < z_1 - \varepsilon$  and  $z_2 + \varepsilon < 1$ . Consider a temperature profile  $T_{\varepsilon}(\mathbf{x}) = T_{\varepsilon}(z)$  that varies only in  $z$  and satisfies

$$\partial_z T_{\varepsilon} := \begin{cases} \varepsilon^{-1} & z_1 - \varepsilon \leq z \leq z_1 + \varepsilon, \\ -\varepsilon^{-1} & z_2 - \varepsilon \leq z \leq z_2 + \varepsilon, \\ 0 & \text{otherwise.} \end{cases}$$

Clearly,  $T_{\varepsilon} \in \mathcal{T}$  and is nonnegative, so the positivity of  $\mathcal{L}_q$  yields

$$0 \leq \mathcal{L}_q\{T_{\varepsilon}\} = - \int_{\Omega} q(z) \partial_z T_{\varepsilon} \, d\mathbf{x} = \frac{1}{\varepsilon} \int_{z_2 - \varepsilon}^{z_2 + \varepsilon} q(z) \, dz - \frac{1}{\varepsilon} \int_{z_1 - \varepsilon}^{z_1 + \varepsilon} q(z) \, dz. \quad (\text{C1})$$

Letting  $\varepsilon \rightarrow 0$  using Lebesgue's differentiation theorem and rearranging yields  $q(z_1) \leq q(z_2)$ , which implies that  $q$  is nondecreasing since  $z_1$  and  $z_2$  are arbitrary.

To prove the reverse statement, suppose that  $q$  is nondecreasing but that  $\mathcal{L}_q$  is not positive. This means that there exist a constant  $c > 0$  and a temperature field  $T_0 \in \mathcal{T}$ , nonnegative on the domain  $\Omega$ , such that  $\mathcal{L}_q(T_0) \leq -c$ . By a standard approximation argument, we may also assume that  $q(z)$  is smooth on  $[0, 1]$ . Then, integration by parts using the boundary conditions on  $T_0$  yields

$$\int_{\Omega} q'(z) T_0 \, d\mathbf{x} = \mathcal{L}_q(T_0) \leq -c.$$

This is a contradiction because the left-hand side is a nonnegative quantity, as  $q'(z) \geq 0$  ( $q$  is nondecreasing) and  $T_0(\mathbf{x}) \geq 0$  on  $\Omega$  by assumption.  $\square$

Lemma 2 guarantees that the bounded linear functional in (4.21) is positive, as required, if  $q$  is nondecreasing. The next result shows that considering more general types of positive linear functionals is not helpful.

**PROPOSITION 2.** *Suppose there exists a positive bounded linear functional  $\mathcal{L} : \mathcal{T} \rightarrow \mathbb{R}$  such that  $\mathcal{S}\{\mathbf{u}, T\} \geq \mathcal{L}\{T\}$  for all pairs  $(\mathbf{u}, T) \in \mathcal{H}$ . Then, there exists a nondecreasing square-integrable function  $q : (0, 1) \rightarrow \mathbb{R}$  such that*

$$\mathcal{S}\{\mathbf{u}, T\} \geq - \int_{\Omega} q(z) \partial_z T \, d\mathbf{x} \quad \forall (\mathbf{u}, T) \in \mathcal{H}. \quad (\text{C2})$$

*Proof.* Since  $\mathcal{T}$  is a Hilbert space and  $\mathcal{L}$  is bounded, the Riesz representation theorem guarantees that there exists a fixed temperature field  $\theta \in \mathcal{T}$  such that

$$\mathcal{L}\{T\} = \int_{\Omega} \nabla \theta \cdot \nabla T \, d\mathbf{x}. \quad (\text{C3})$$

Next, fix any pair  $(\mathbf{u}, T) \in \mathcal{H}$  and observe that, by virtue of the horizontal periodicity, the pair of translated fields  $(\mathbf{u}_{r,s}, T_{r,s}) := (\mathbf{u}(x+r, y+s, z), T(x+r, y+s, z))$  also belongs to  $\mathcal{H}$ . By assumption  $\mathcal{S}\{\mathbf{u}, T\} \geq \mathcal{L}\{T\}$  for all  $(\mathbf{u}, T) \in \mathcal{H}$ , so

$$\mathcal{S}\{\mathbf{u}_{r,s}, T_{r,s}\} \geq \int_{\Omega} \nabla \theta \cdot \nabla T_{r,s} \, d\mathbf{x} = \int_{\Omega} \nabla \theta_{-r,-s} \cdot \nabla T \, d\mathbf{x}, \quad (\text{C } 4)$$

where the second equality follows from a change of variables. The same change of variables shows that  $\mathcal{S}\{\mathbf{u}_{r,s}, T_{r,s}\} = \mathcal{S}\{\mathbf{u}, T\}$ , so averaging (C 4) over all horizontal shifts  $r$  and  $s$  yields

$$\mathcal{S}\{\mathbf{u}, T\} \geq \int_{\Omega} \nabla \bar{\theta} \cdot \nabla T \, d\mathbf{x} = \int_{\Omega} \bar{\theta}'(z) \partial_z T \, d\mathbf{x}. \quad (\text{C } 5)$$

The expression on right-hand side of this inequality is a positive linear functional because it is the average of the positive functionals  $T \rightarrow \mathcal{L}\{T_{r,s}\}$ . Since the pair  $(\mathbf{u}, T) \in \mathcal{H}$  is arbitrary, inequality (C 2) follows upon setting  $q(z) := -\bar{\theta}'(z)$  and applying Lemma 2 to conclude that  $q$  is nondecreasing and square-integrable.  $\square$

## Appendix D. Computational approach

The optimisation problems (4.12) and (4.25) can be discretised into SDPs following a general strategy, and then solved using efficient algorithms for convex optimisation. This “discretise-then-optimise” approach preserves the linearity of the original infinite-dimensional problems and enables one to readily impose additional constraints, such as the inequalities on  $\psi(0)$ ,  $\psi(1)$  and the monotonicity constraint on  $q$ , that are not easy to enforce following “optimise-then-discretise” strategies based on the numerical solution of the Euler–Lagrange equations for (4.12) and (4.25).

The discretisation process starts by approximating the tunable functions  $\psi$ ,  $q$  and the unknown fields  $\hat{T}_0$ ,  $\hat{T}_{\mathbf{k}}$  and  $\hat{w}_{\mathbf{k}}$  using a finite set of basis functions  $\{\Phi_1(z), \dots, \Phi_n(z)\}$ , e.g.,

$$\psi(z) = \sum_{i=1}^n A_i \Phi_i(z). \quad (\text{D } 1)$$

Here we use a single set of basis functions for simplicity, but different fields could be approximated using different bases to improve accuracy or allow for varying degrees of smoothness. Note that while the functions  $\psi$  and  $q$  are arbitrary, so we are free to choose such a finite-dimensional representation without much loss of generality, assuming the same for the test functions  $\hat{T}_0$ ,  $\hat{T}_{\mathbf{k}}$  and  $\hat{w}_{\mathbf{k}}$  represents a relaxation of the constraints in (4.12) and (4.25). Strictly speaking, therefore, our numerical results are not rigorous upper bounds on the vertical heat flux, but we expect convergence as  $n \rightarrow \infty$ .

Substituting expansions such as (D 1) into the inequalities on  $\mathcal{S}_0$  and  $\tilde{\mathcal{S}}$  in (4.12) and (4.25) reduces them to quadratic polynomial inequalities, where the independent variables are the (unknown) expansion coefficients of  $\hat{T}_0$ ,  $\hat{T}_{\mathbf{k}}$  and  $\hat{w}_{\mathbf{k}}$ , and the coefficients depend linearly on the optimisation variables—the scalars  $U$ ,  $a$ ,  $b$  and the expansion coefficients of  $\psi$  and  $q$ . These quadratic polynomial inequalities are equivalent to positive semidefiniteness constraints on matrices that depend linearly on the polynomial coefficients, and hence on the optimisation variables. Moreover, the inequalities  $\psi(0) \leq 1$ ,  $\psi(1) \leq 0$  and the monotonicity constraint on  $q(z)$  in (4.25) can be projected onto the expansion basis to obtain a set of linear constraints on the expansion coefficients of  $\psi$  and  $q$ . The discrete problems are therefore SDPs (Boyd & Vandenberghe 2004) and can be solved with a variety of algorithms (see, e.g., Nemirovski 2006).

To tackle (4.12) and (4.25), we used a finite-element approximation similar to that considered by Fantuzzi *et al.* (2018). The reason for this choice is twofold. First, a piecewise-linear finite-element representation for  $q$  enables us to impose exactly the monotonicity constraint, which is key to enforcing the minimum principle on the temperature as discussed in §4.4. Second, the optimal  $\psi$  and  $q$  have steep boundary layers near the bottom boundary that cannot be approximated accurately at a reasonable computational cost using global polynomial expansions (e.g. Legendre series). Finite-element bases, instead, lead to SDPs with so-called *chordal sparsity* (Fukuda *et al.* 2001) that can be solved extremely efficiently. For our particular problem, however, we also found that finite-element bases lead to SDPs with worse numerical conditioning than those obtained with other bases, such as Legendre polynomials. Accurate solution, therefore, required the multiple-precision solver SDPA-GMP (Fujisawa *et al.* 2008; Waki *et al.* 2012). Despite this issue, which we do not expect to be generic, the enhanced sparsity of the finite-element approach resulted in significant efficiency gains compared to accurate Legendre series expansions.

## Appendix E. Estimates on the spectral constraint

A  $R$  dependent variation of the parameters follows from enforcing the spectral constraint. In the bulk of the domain the constraint can easily be satisfied for any profile  $\psi(z)$  such that  $\psi'(z) = a$  for  $z \in (\delta, 1 - \varepsilon)$ . With this assumption, the only sign-indefinite term in (4.11) is

$$\int_0^1 (a - \psi') \hat{w}_{\mathbf{k}} \hat{T}_{\mathbf{k}} dz = \int_{[0, \delta] \cup [1 - \varepsilon, 1]} (a - \psi') \hat{w}_{\mathbf{k}} \hat{T}_{\mathbf{k}} dz. \quad (\text{E } 1)$$

Where we take the real part of the product  $\hat{w}_{\mathbf{k}} \hat{T}_{\mathbf{k}}^*$ . To estimate the integral over  $[0, \delta]$ , we apply the fundamental theorem of calculus, the boundary condition  $\hat{w}_{\mathbf{k}}(0) = 0$  and the Cauchy–Schwarz inequality to bound

$$w(z) = \int_0^z w'(\xi) d\xi \leq \sqrt{z} \|w'_{\mathbf{k}}\|_2, \quad (\text{E } 2)$$

$$w(z) \leq \frac{1}{\sqrt{2}} z^{\frac{3}{2}} \|w''_{\mathbf{k}}\|_2. \quad (\text{E } 3)$$

Identical estimates show that  $T(z) \leq \sqrt{z} \|T'_{\mathbf{k}}\|_2$ . Using these inequalities, we can estimate in two ways such that

$$\begin{aligned} \left| \int_0^\delta (a - \psi') \hat{w}_{\mathbf{k}} \hat{T}_{\mathbf{k}} dz \right| &\leq \|a - \psi'\|_{L^\infty(0, \delta)} \int_0^\delta |\hat{w}_{\mathbf{k}}| |\hat{T}_{\mathbf{k}}| dz \\ &\leq \delta^2 \|a - \psi'\|_{L^\infty(0, \delta)} \left( \frac{\alpha}{2} \|\hat{w}'_{\mathbf{k}}\|_2 \|\hat{T}'_{\mathbf{k}}\|_2 + \frac{1 - \alpha}{2\sqrt{2}} \|\hat{w}''_{\mathbf{k}}\|_2 \|\hat{T}_{\mathbf{k}}\|_2 \right). \end{aligned} \quad (\text{E } 4)$$

where  $\alpha \in [0, 1]$  is a weighting parameter to be specified later. Similar analysis near  $z = 1$  yields

$$\left| \int_{1 - \varepsilon}^1 (a - \psi') \hat{w}_{\mathbf{k}} \hat{T}_{\mathbf{k}} dz \right| \leq \varepsilon^2 \|a - \psi'\|_{L^\infty(1 - \varepsilon, 1)} \left( \frac{\beta}{2} \|\hat{w}'_{\mathbf{k}}\|_2 \|\hat{T}'_{\mathbf{k}}\|_2 + \frac{1 - \beta}{2\sqrt{2}} \|\hat{w}''_{\mathbf{k}}\|_2 \|\hat{T}_{\mathbf{k}}\|_2 \right), \quad (\text{E } 5)$$

again  $\beta \in [0, 1]$  is a weighting parameter. Substituting inequalities (E 4) and (E 5) into (4.11) shows that

$$\begin{aligned} \mathcal{S}_k &\geq \frac{2a}{R} \|\hat{w}'_k\|_2^2 - \frac{1}{2} \lambda_1(a, \delta, \varepsilon, \alpha, \beta, \psi') \|\hat{w}'_k\|_2 \|\hat{T}'_k\|_2 + b \|\hat{T}'_k\|_2^2 \\ &\quad + \frac{a}{Rk^2} \|\hat{w}''_k\|_2^2 - \frac{1}{2\sqrt{2}} \lambda_2(a, \delta, \varepsilon, \alpha, \beta, \psi') \|\hat{w}''_k\|_2 \|\hat{T}_k\|_2 + bk^2 \|\hat{T}_k\|_2^2 \end{aligned} \quad (\text{E } 6)$$

where

$$\lambda_1(a, \delta, \varepsilon, \alpha, \beta, \psi') := \alpha \delta^2 \|a - \psi'\|_{L^\infty(0, \delta)} + \beta \varepsilon^2 \|a - \psi'\|_{L^\infty(1-\varepsilon, 1)}, \quad (\text{E } 7)$$

$$\lambda_2(a, \delta, \varepsilon, \alpha, \beta, \psi') := (1 - \alpha) \delta^2 \|a - \psi'\|_{L^\infty(0, \delta)} + (1 - \beta) \varepsilon^2 \|a - \psi'\|_{L^\infty(1-\varepsilon, 1)}. \quad (\text{E } 8)$$

The right-hand side of the last inequality is two homogeneous quadratic forms in the variables  $\|\hat{w}'_k\|_2$ ,  $\|\hat{T}'_k\|_2$  and  $\|\hat{w}''_k\|_2$ ,  $\|\hat{T}_k\|_2$ , so it is nonnegative if the discriminant of both forms is nonpositive, i.e.,

$$|\lambda_1(a, \delta, \varepsilon, \alpha, \beta, \psi')|^2 \leq \frac{32ab}{R}, \quad (\text{E } 9)$$

$$|\lambda_2(a, \delta, \varepsilon, \alpha, \beta, \psi')|^2 \leq \frac{32ab}{R}, \quad (\text{E } 10)$$

from which it is obvious that  $\alpha = \beta = 1/2$  is optimal. Then it suffices to take square roots and rearrange, such that we conclude that  $\mathcal{S}_k \geq 0$  if

$$\delta^2 \|a - \psi'\|_{L^\infty(0, \delta)} + \varepsilon^2 \|a - \psi'\|_{L^\infty(1-\varepsilon, 1)} \leq \frac{8\sqrt{2ab}}{\sqrt{R}}. \quad (\text{E } 11)$$

This condition reduces to (5.3) when  $\delta = \varepsilon$  and  $\psi$  is as in (5.1).

## Appendix F. Proof of Proposition 1

It is assumed that  $(a, b, \psi, q) \in \mathcal{A}\{\delta, \varepsilon\} \cap \mathcal{B}\{\gamma\} \cap \mathcal{C}\{\delta, \varepsilon, R\}$ . The first step is to bound  $\int_0^1 \psi(z) dz$  from above. To do this, we work back from  $z = 1$ , using the assumptions to estimate  $\psi$ .

Let  $1 - \varepsilon \leq z \leq 1$ . Since  $\psi \in C^1[0, 1]$  and  $\psi(1) = 0$ , the mean value theorem implies that there exist  $z_\varepsilon \in (1 - \varepsilon, 1)$  such that

$$-\psi'(z_\varepsilon) = \frac{\psi(z)}{1 - z} \geq \frac{\psi(z)}{\varepsilon}.$$

Since  $(a, b, \psi(z))$  satisfy (E 11), it follows that

$$\begin{aligned} \varepsilon^4 \|a - \psi'\|_{L^\infty(1-\varepsilon, 1)}^2 &\leq 128 \frac{ab}{R} \implies \varepsilon^4 \left( a + \frac{\psi(z)}{\varepsilon} \right)^2 \leq 128 \frac{ab}{R} \\ &\implies \varepsilon^4 \left( \frac{a}{b} \right)^2 + \left( \frac{a}{b} \right) \left( \frac{2\varepsilon^3 \psi(z)}{b} - \frac{128}{R} \right) + \left( \frac{\varepsilon \psi(z)}{b} \right)^2 \leq 0 \\ &\implies \left( \frac{2\varepsilon^3 \psi(z)}{b} - \frac{128}{R} \right)^2 \geq 4\varepsilon^4 \left( \frac{\varepsilon \psi(z)}{b} \right)^2 \\ &\implies \frac{\psi(z) \varepsilon^3}{b} \leq \frac{32}{R} \end{aligned} \quad (\text{F } 1)$$



Next, since  $\psi(1) = 0$ , the assumption that  $\|\psi'\|_{L^\infty(1-\varepsilon,1)} \leq 2b$  gives  $|\psi(z)| \leq \varepsilon\|\psi'\|_{L^\infty(1-\varepsilon,1)} \leq 2b\varepsilon$ , which in turn implies

$$\varepsilon \geq \frac{1}{2b}\psi(z). \quad (\text{F } 2)$$

Since  $1 - \varepsilon < z < 1$  was arbitrary in the above argument, it follows from (F 1) and (F 2) and the fact that  $\psi'(z) \geq 0$  for all  $z \in [\delta, 1 - \varepsilon]$  that

$$\|\psi\|_{L^\infty(\delta,1)} \leq \|\psi\|_{L^\infty(1-\varepsilon,1)} \leq 4bR^{-\frac{1}{4}}. \quad (\text{F } 3)$$

We now estimate  $\psi$  in the lower boundary layer  $[0, \delta]$ . The mean value theorem implies that there exists  $z_\delta$  such that

$$\psi'(z_\delta) = \frac{\psi(\delta) - \psi(0)}{\delta}.$$

Since  $(a, b, \psi(z))$  satisfy (E 11), using the above equation and the assumption that  $0 < a \leq b$ , it then follows that

$$\begin{aligned} \delta^4 \|a - \psi'\|_{L^\infty(0,\delta)}^2 &\leq 128 \cdot \frac{ab}{R} \implies \delta^4 \left| a + \left( \frac{\psi(0) - \psi(\delta)}{\delta} \right) \right|^2 \leq 128 \cdot \frac{ab}{R} \\ &\implies \delta^2 |a\delta + \psi(0) - \psi(\delta)|^2 \leq 128 \cdot \frac{b^2}{R} \\ &\implies \frac{\delta}{b} \psi(0) \leq \frac{8\sqrt{2}}{R^{\frac{1}{2}}} + \frac{\delta\psi(\delta)}{b} \\ (\text{by (F 3)}) \implies \frac{\delta}{b} \psi(0) &\leq \frac{8\sqrt{2}}{R^{\frac{1}{2}}} + \frac{4\delta}{R^{\frac{1}{4}}} \end{aligned} \quad (\text{F } 4)$$

Using (F 3), (F 4), the assumption that  $\psi'(z) \leq 0$  on  $[0, \delta]$  and  $R \geq 1$  gives

$$\frac{1}{b} \int_0^1 \psi(z) dz \leq \frac{\delta}{b} \psi(0) + \frac{(1-\delta)}{b} \|\psi\|_{L^\infty(\delta,1)} \leq \frac{8\sqrt{2} + 4}{R^{\frac{1}{4}}} \quad (\text{F } 5)$$

Next we consider the  $L^2$  component of the cost function. Using the assumption that  $\psi', q$  are constant in an interval  $(1/2 - \gamma, 1/2 + \gamma)$ ,

$$\begin{aligned} \frac{1}{4b} \|\psi' - q - b(z - 1/2)\|_2^2 &\geq \frac{1}{4b} \int_{\frac{1}{2}-\gamma}^{\frac{1}{2}+\gamma} [\psi' - q - b(z - 1/2)]^2 dz \\ &\geq \frac{b}{4} \int_{\frac{1}{2}-\gamma}^{\frac{1}{2}+\gamma} (z - 1/2)^2 dz \\ &= \frac{b\gamma^3}{6}. \end{aligned} \quad (\text{F } 6)$$

Combining the above estimate with (F 5) gives the stated result

$$\frac{1}{4b} \|\psi' - q - b(z - 1/2)\|_2^2 - \int_0^1 \psi(z) dz \geq \frac{b}{6} \left( \gamma^3 - 24 \cdot \frac{1 + 2\sqrt{2}}{R^{\frac{1}{4}}} \right).$$

## REFERENCES

BERCOVICI, D. 2011 Mantle convection. *Encyclopedia of Solid Earth Geophysics*. Gupta, HK, (ed.) Springer .

- BOUILLAUT, VINCENT, LEPOT, SIMON, AUMAÎTRE, SÉBASTIEN & GALLET, BASILE 2019 Transition to the ultimate regime in a radiatively driven convection experiment. *Journal of Fluid Mechanics* **861**, R5.
- BOYD, S. & VANDENBERGHE, L. 2004 *Convex Optimization*. Cambridge University Press.
- CHERNYSHENKO, S. I. 2017 Relationship between the methods of bounding time averages. *arXiv preprint arXiv:1704.02475* .
- CHERNYSHENKO, S. I., GOULART, P. J., HUANG, D. & PAPACHRISTODOULOU, A. 2014 Polynomial sum of squares in fluid dynamics: a review with a look ahead. *Philosophical Transactions of the Royal Society A: Mathematical, Physical and Engineering Sciences* **372** (2020), 20130350.
- CHOFFRUT, A., NOBILI, C. & OTTO, F. 2016 Upper bounds on Nusselt number at finite Prandtl number. *Journal of Differential Equations* **260** (4), 3860–3880.
- CONSTANTIN, P. & DOERING, C. R. 1995 Variational bounds on energy dissipation in incompressible flows. II. Channel flow. *Physical Review E* **51** (4), 3192.
- CONSTANTIN, P. & DOERING, C. R. 1996 Heat transfer in convective turbulence. *Nonlinearity* **9** (4), 1049–1060.
- CONSTANTIN, P. & DOERING, C. R. 1999 Infinite Prandtl number convection. *Journal of Statistical Physics* **94** (1-2), 159–172.
- DEBLER, W. R. 1959 The onset of laminar natural convection in a fluid with homogeneously distributed heat sources. PhD thesis, University of Michigan.
- DOERING, C. R. & CONSTANTIN, P. 1994 Variational bounds on energy dissipation in incompressible flows: shear flow. *Physical Review E* **49** (5), 4087.
- DOERING, C. R. & CONSTANTIN, P. 1996 Variational bounds on energy dissipation in incompressible flows. III. Convection. *Physical Review E* **53** (6), 5957.
- DOERING, C. R. & CONSTANTIN, P. 1998 Bounds for heat transport in a porous layer. *Journal of Fluid Mechanics* **376**, 263–296.
- DOERING, C. R. & CONSTANTIN, P. 2001 On upper bounds for infinite Prandtl number convection with or without rotation. *Journal of Mathematical Physics* **42** (2), 784–795.
- DOERING, C. R., OTTO, F. & REZNIKOFF, M. G. 2006 Bounds on vertical heat transport for infinite-Prandtl-number Rayleigh–Bénard convection. *Journal of fluid mechanics* **560**, 229–241.
- EMARA, A. A. & KULACKI, F. A. 1980 A numerical investigation of thermal convection in a heat-generating fluid layer. *Journal of Heat Transfer* **102** (3), 531–537.
- FANTUZZI, G., GOLUSKIN, D., HUANG, D. & CHERNYSHENKO, S. I. 2016 Bounds for deterministic and stochastic dynamical systems using sum-of-squares optimization. *SIAM Journal on Applied Dynamical Systems* **15** (4), 1962–1988.
- FANTUZZI, G., PERSHIN, A. & WYNN, A. 2018 Bounds on heat transfer for Bénard–Marangoni convection at infinite Prandtl number. *Journal of Fluid Mechanics* **837**, 562–596.
- FANTUZZI, G. & WYNN, A. 2015 Construction of an optimal background profile for the Kuramoto–Sivashinsky equation using semidefinite programming. *Physics Letters A* **379** (1-2), 23–32.
- FANTUZZI, G. & WYNN, A. 2016 Optimal bounds with semidefinite programming: An application to stress-driven shear flows. *Physical Review E* **93** (4), 043308.
- FANTUZZI, G., WYNN, A., GOULART, P. J. & PAPACHRISTODOULOU, A. 2017 Optimization with affine homogeneous quadratic integral inequality constraints. *IEEE Transactions on Automatic Control* **62** (12), 6221–6236.
- FOIAS, C., MANLEY, O. & TEMAM, R. 1987 Attractors for the Bénard problem: existence and physical bounds on their fractal dimension. *Nonlinear Analysis: Theory, Methods & Applications* **11** (8), 939–967.
- FUJISAWA, K., FUKUDA, M., KOBAYASHI, K., KOJIMA, M., NAKATA, K., NAKATA, M. & YAMASHITA, M. 2008 SDPA (SemiDefinite Programming Algorithm) and SDPA-GMP User’s Manual – Version 7.1.1. *Tech. Rep.*. Department of Mathematical and Computing Sciences, Tokyo Institute of Technology, Tokyo, Japan.
- FUJISAWA, KATSUKI, KIM, SUNYOUNG, KOJIMA, MASAKAZU, OKAMOTO, Y. & YAMASHITA, MAKOTO 2009 User’s Manual for SparseCoLO: Conversion Methods for SPARSE CONic-form Linear Optimization Problems. *Tech. Rep.*. Department of Mathematical and Computing Sciences, Tokyo Institute of Technology, Tokyo, Japan.

- FUKUDA, M., KOJIMA, M., MUROTA, K. & NAKATA, K. 2001 Exploiting sparsity in semidefinite programming via matrix completion I: General framework. *SIAM Journal on Optimization* **11** (3), 647–674.
- GOLUSKIN, D. 2015 Internally heated convection beneath a poor conductor. *Journal of Fluid Mechanics* **771**, 36–56.
- GOLUSKIN, D. 2016 *Internally heated convection and Rayleigh–Bénard convection*. Springer.
- GOLUSKIN, D. & DOERING, C. R. 2016 Bounds for convection between rough boundaries. *Journal of Fluid Mechanics* **804**, 370–386.
- GOLUSKIN, D. & FANTUZZI, G. 2019 Bounds on mean energy in the Kuramoto-Sivashinsky equation computed using semidefinite programming. *Nonlinearity* **32** (5), 1705–1730.
- GOLUSKIN, D. & VAN DER POEL, E. P. 2016 Penetrative internally heated convection in two and three dimensions. *Journal of Fluid Mechanics* **791**.
- GOLUSKIN, D. & SPIEGEL, E. A. 2012 Convection driven by internal heating. *Physics Letters A* **377** (1-2), 83–92.
- GROSSMANN, S. & LOHSE, D. 2000 Scaling in thermal convection: a unifying theory. *Journal of Fluid Mechanics* **407**, 27–56.
- HOWARD, L. N. 1961 Note on a paper of John W. Miles. *Journal of Fluid Mechanics* **10** (4), 509–512.
- JAHN, M. & REINEKE, H.-H. 1974 Free convection heat transfer with internal heat sources, calculations and measurements. In *Proceedings of the 5<sup>th</sup> International Heat Transfer Conference*, pp. 74–78. Tokyo.
- KAKAC, S., AUNG, W. M. & VISKANTA, R. 1985 Natural convection: fundamentals and applications. *Washington, DC, Hemisphere Publishing Corp., 1985, 1191 p.*
- KULACKI, F. A. & GOLDSTEIN, R. J. 1972 Thermal convection in a horizontal fluid layer with uniform volumetric energy sources. *Journal of Fluid Mechanics* **55** (2), 271–287.
- LEE, S. D., LEE, J. K. & SUH, K. Y. 2007 Boundary condition dependent natural convection in a rectangular pool with internal heat sources. *Journal of Heat Transfer* **129** (5), 679–682.
- LU, L., DOERING, C. R. & BUSSE, F. H. 2004 Bounds on convection driven by internal heating. *Journal of mathematical physics* **45** (7), 2967–2986.
- MALKUS, W. V. R. 1954 The heat transport and spectrum of thermal turbulence. *Proceedings of the Royal Society of London. Series A. Mathematical and Physical Sciences* **225** (1161), 196–212.
- MAYINGER, F., JAHN, M., REINEKE, H. & STEIBNER, V. 1976 Examination of thermohydraulic processes and heat transfer in a core melt. *Tech. Rep. BMFT RS 48/1*. Institut für Verfahrenstechnik der TU, Hanover Germany.
- MILES, J. W. 1961 On the stability of heterogeneous shear flows. *Journal of Fluid Mechanics* **10** (4), 496–508.
- NEMIROVSKI, A. 2006 Advances in convex optimization: Conic programming. In *International Congress of Mathematicians*, , vol. 1, pp. 413–444.
- OTERO, J., DONTCHEVA, L. A., JOHNSTON, H., WORTHING, R. A., KURGANOV, A., PETROVA, G. & DOERING, C. R. 2004 High-Rayleigh-number convection in a fluid-saturated porous layer. *Journal of Fluid Mechanics* **500**, 263–281.
- OTERO, J., WITTENBERG, R. W., WORTHING, R. A. & DOERING, C. R. 2002 Bounds on Rayleigh–Bénard convection with an imposed heat flux. *Journal of Fluid Mechanics* **473**, 191–199.
- OTTO, F. & SEIS, C. 2011 Rayleigh–Bénard convection: improved bounds on the Nusselt number. *Journal of mathematical physics* **52** (8), 083702.
- PECKOVER, R. S. & HUTCHINSON, I. H. 1974 Convective rolls driven by internal heat sources. *Physics of Fluids* **17** (7), 1369–1371.
- PLASTING, S. C. & KERSWELL, R. R. 2003 Improved upper bound on the energy dissipation rate in plane Couette flow: the full solution to Busse’s problem and the Constantin-Doering-Hopf problem with one-dimensional background field. *Journal of Fluid Mechanics* **477**, 363–379.
- PRIESTLEY, C. H. B. 1954 Vertical heat transfer from impressed temperature fluctuations. *Australian Journal of Physics* **7** (1), 202–209.
- ROSA, R. & TEMAM, R. M. 2020 Optimal minimax bounds for time and ensemble averages

- of dissipative infinite-dimensional systems with applications to the incompressible navier-stokes equations. *arXiv preprint arXiv:2010.06730* .
- SPIEGEL, E. A. 1963 A generalization of the mixing-length theory of turbulent convection. *The Astrophysical Journal* **138**, 216.
- STRAUS, J. M. 1976 Penetrative convection in a layer of fluid heated from within. *The Astrophysical Journal* **209**, 179–189.
- TILGNER, A. 2017 Bounds on poloidal kinetic energy in plane layer convection. *Physical Review Fluids* **2** (12), 123502.
- TILGNER, A. 2019 Time evolution equation for advective heat transport as a constraint for optimal bounds in Rayleigh-Bénard convection. *Physical Review Fluids* **4** (1), 1–11.
- TOBASCO, I., GOLUSKIN, D. & DOERING, C. R. 2018 Optimal bounds and extremal trajectories for time averages in nonlinear dynamical systems. *Physics Letters A* **382** (6), 382–386.
- TRITTON, D. J. 1975 Internally heated convection in the atmosphere of venus and in the laboratory. *Nature* **257** (5522), 110–112.
- TROWBRIDGE, A. J., MELOSH, H. J., STECKLOFF, J. K. & FREED, A. M. 2016 Vigorous convection as the explanation for Pluto’s polygonal terrain. *Nature* **534** (7605), 79–81.
- TVEITEREID, M. 1978 Thermal convection in a horizontal fluid layer with internal heat sources. *International Journal of Heat and Mass Transfer* **21** (3), 335–339.
- WAKI, H., NAKATA, M. & MURAMATSU, M. 2012 Strange behaviors of interior-point methods for solving semidefinite programming problems in polynomial optimization. *Computational Optimization and Applications* **53** (3), 823–844.
- WANG, Q., LOHSE, D. & SHISHKINA, O. 2020 Scaling in internally heated convection: a unifying theory. *Geophysical Research Letters* **47**, e2020GL091198.
- WEN, B., CHINI, G. P., DIANATI, N. & DOERING, C. R. 2013 Computational approaches to aspect-ratio-dependent upper bounds and heat flux in porous medium convection. *Physics Letters A* **377** (41), 2931–2938.
- WEN, B., CHINI, G. P., KERSWELL, R. R. & DOERING, C. R. 2015 Time-stepping approach for solving upper-bound problems: Application to two-dimensional Rayleigh-Bénard convection. *Physical Review E* **92** (4), 043012.
- WHITEHEAD, J. P. & DOERING, C. R. 2011a Internal heating driven convection at infinite Prandtl number. *Journal of mathematical physics* **52** (9), 093101.
- WHITEHEAD, J. P. & DOERING, C. R. 2011b Ultimate State of Two-Dimensional Rayleigh-Bénard Convection between Free-Slip Fixed-Temperature Boundaries. *Physical Review Letters* **106** (24), 244501.
- WHITEHEAD, J. P. & DOERING, C. R. 2012 Rigid bounds on heat transport by a fluid between slippery boundaries. *Journal of Fluid Mechanics* **707**, 241–259.
- WÖRNER, M., SCHMIDT, M. & GRÖTZBACH, G. 1997 Direct numerical simulation of turbulence in an internally heated convective fluid layer and implications for statistical modelling. *Journal of Hydraulic Research* **35** (6), 773–797.
- YAMASHITA, M., FUJISAWA, K., FUKUDA, M., KOBAYASHI, K., NAKATA, K. & NAKATA, M. 2012 Latest developments in the sdpa family for solving large-scale sdps. In *Handbook on semidefinite, conic and polynomial optimization*, pp. 687–713. Springer.
- YAN, X. 2004 On limits to convective heat transport at infinite Prandtl number with or without rotation. *Journal of Mathematical Physics* **45** (7), 2718–2743.